J Ther Eng, Vol. 12, No. 1, pp. 156−181, January, 2026

Journal of Thermal Engineering
Web page info: https://jten.yildiz.edu.tr
DOI: 10.14744/thermal.0001067

Research Article

Turbulent forced convection of hybrid nanofluids in a three-dimensional L-shaped channel: Modeling, analysis, and regression model development

Amanullah PHULPOTO[1], Abid A. MEMON[1], M. Asif MEMON[1,*], Ubaidullah YASHKUN[1], Adebowale Martins OBALALU[2]

[1]*Department of Mathematics, Basic Sciences and Humanities, Sukkur IBA University, Sukkur, 65200, Sindh, Pakistan*
[2]*Department of Mathematics and Statistics, Kwara State University, Malete, 241103, Nigeria*

ARTICLE INFO

Article history
Received: 20 September 2024
Revised: 19 December 2024
Accepted: 23 December 2024

Keywords:
Convection; Darcy; Kinetic Energy; L-shaped Channel; Turbulent

ABSTRACT

The study explores turbulent forced convection of hybrid nanofluids in a three-dimensional L-shaped channel using COMSOL Multiphysics. The hybrid nanofluid comprises copper and aluminum oxide particles dispersed in water, with volume fractions of 0.01 (1%), 0.04 (4%), 0.07 (7%), and 0.1 (10%). Simulations are conducted for forced convection under Reynolds numbers ranging from 10,000 to 40,000. The partial differential equations of the Navier-Stokes, $\kappa - \varepsilon$ model of the turbulence, and the three-dimensional energy equation are employed to model the system. The turbulence kinetic energy and dissipation rates for the turbulent flow range from 2.99E-3 to 1.53 (m^2 / s^2) and from 0.2136 to 2524.1913 (m^3 / s^3), respectively. This research is significant for advancing efficient heat transfer mechanisms, which are crucial for applications in cooling systems and energy devices. Key findings include the observation that the minimum temperature at the channel edges decreases with an increasing volume fraction of aluminum oxide and improves with copper addition. Copper consistently enhances the minimum temperature across all scenarios. The Nusselt number calculated using aluminum oxide is nearly ten times greater than that obtained using copper. The friction factor initially increases along the channel length and then decreases, showing minimal sensitivity to variations in the volume fractions of copper and aluminum oxide. Using multiple linear regression, predictive equations for the average temperature and Nusselt number at the outlet were developed based on the Reynolds number and the nanomaterial volume fractions. The novelty of this work lies in the exploration of a three-dimensional L-shaped channel to analyze its thermal behavior, offering significant insights for engineering applications and design improvements. Furthermore, the study provides a novel contribution by deriving linear regression equations for the average Nusselt number and average temperature, which have not been addressed in previous literature. The absolute error for the average temperature equation ranges from 0.005 to 1.6, while for the Nusselt number, it varies between 0.368 and 1.6, ensuring high accuracy of the regression model.

Cite this article as: Phulpoto A, Memon AA, Memon MA, Yashkun U, Obalalu AM. Turbulent forced convection of hybrid nanofluids in a three-dimensional l-shaped channel: Modeling, analysis, and regression model development. J Ther Eng 2026;12(1):156−181.

***Corresponding author.**
*E-mail address: asif-memon@iba-suk.edu.pk

This paper was recommended for publication in revised form by Editor-in-Chief Ahmet Selim Dalkilic

INTRODUCTION

Heat transfer in fluid dynamics plays a significant role in optimizing solutions in the industrial sector [1-3]. Many practical applications of heat transfer are found in industries to enhance energy production and develop efficient heat exchangers [4-6] and [7-10]. Heat transfer is also crucial in the design of efficient solar collectors, and sometimes, the use of porous materials can further improve heat transfer [11-14] and [15, 16]. Initially, the focus was on using conventional fluids like ethylene glycol, oil, and water to achieve efficient heat transfer. The second approach involved incorporating metallic particles with high thermal conductivity to enhance heat transfer rates. To explore this second idea, researchers conducted an experiment involving the transport of metallic particles through conventional fluids to assess thermal performance [17]. The results of this experiment demonstrated that the transport of nanofluids significantly enhances heat transfer rates. Following this breakthrough, numerous experiments were conducted to fully harness the potential of nanofluid transportation. Many research articles have been published proposing methods to control the rate of heat energy distribution through the transport of nanofluids. Initially, only individual types of nanoparticles, such as copper, aluminum oxide, magnesium oxide, and copper oxide, were mixed with the base fluid to enhance heat transfer. Numerous research papers and experiments have explored optimizing heat transfer using various approaches, such as applying electric and magnetic fields and examining the effects of different nanoparticle shapes [18-20]. Scientists and researchers dedicated nearly two decades to investigating and enhancing heat transfer until the third idea emerged. The third idea involves using hybrid fluids, where a mixture of multiple nanoparticles is dispersed in the fluid to further enhance heat transfer efficiency.

Owing to its excellent thermo-physical properties, the hybrid mixture yields remarkable results for heat transfer [21]. The combination of Al_2O_3 and multi-walled carbon nanotubes was selected to be suspended in oil as the base fluid, flowing through the channel [21]. This was done at volume fractions of 0.125% and 1.5%, under ideal conditions while maintaining temperatures of 25°C and 30°C. The uniformity of the mixture was assessed using the zeta potential tool. The study evaluated whether the flow was laminar or turbulent and found that all thermal properties, including pumping power, thermal conductivity, and convection, increased with the hybrid mixture's volume fraction. Furthermore, this study established a significant correlation based on the viscosity of the mixture and its thermal conductivity, referencing available data. Another investigation involved the transport of Al_2O_3 and copper in water as the base fluid, within an open cavity, using the principles of entropy and mixed convection [22]. Researchers analyzed the heat transfer within the cavity while maintaining three adiabatic walls. The study evaluated the effects using three non-dimensional parameters (Rayleigh number (Ra), Hartmann number Ha and nanoparticles voluem fraction ϕ). It was observed that the average Nusselt number and entropy had an inverse relationship with the Hartmann number. Additionally, the heat transfer rate increased with the rise in the Richardson number and entropy production. In a separate analysis, a porous cavity was studied under natural convection conditions, with the transport of copper and aluminum oxide driven by magnetic interactions across the entire domain [23]. The partial differential equations were discretized using the finite difference method along with upwind terms. The primary finding indicated that the average Nusselt number decreased when shifting the heat source. It was also noted that the Hartmann number negatively affected the speed of the hybrid mixture. Furthermore, the study clarified that the Nusselt number remained positive with varying volume fractions.

Researchers studied heat transfer within the cavity while maintaining three adiabatic walls. In some articles [24, 25], oil was used as the base fluid. In other studies, the investigation focused on using oil as the base fluid to comprehensively examine the convection process within the domain of interest [26-30]. Another convection problem was studied involving the flow of a mixture composed of 95% aluminum and 5% zinc, employing a two-step numerical approach under steady-state conditions [31]. Similarly, various studies have explored the heat dispersion process using hybrid nanofluids, with some utilizing ethylene glycol as the working fluid [32-34]. Various geometries have been explored in the past to optimize heat transfer rates when transporting hybrid mixtures. The flow of hybrid nanofluids has been investigated in L-shaped channels [35], three-dimensional U-shaped channels [36], lid-driven channels [37], square channels with various obstacles [38], triangular cavities [39], and backward-facing step channels [40]. These numerical and experimental investigations have aimed to enhance heat transfer rates in different flow conditions, whether laminar or turbulent. These studies have considered both transient and steady-state flows, with the majority utilizing numerical simulations or experimental approaches.

The study conducted a numerical investigation of turbulent natural convection within a square cavity with heat-conducting walls, thermal radiation, and a heat source [41, 42]. It utilized a finite difference method and k–ε turbulence model to simulate heat and mass transfer. Increased surface emissivity and thermal conductivity ratio generally enhanced the average total Nusselt number. However, higher surface emissivity alone reduced the average convective Nusselt number. The study conducted numerical simulations of turbulent natural convection with thermal radiation in an inclined square enclosure with a heat source [42]. It focused on the effect of the inclination angle on fluid flow and heat transfer. Using the k–ε turbulence model and finite difference method, the study considered various parameters including Rayleigh number, inclination angle,

and surface emissivity. Results showed that increasing the inclination angle reduced the radiative Nusselt number. The objective of the project was to apply computational modeling to improve energy transport in engineering applications [43]. Research was done on turbulent forced convective energy transmission in a curved channel where the intake offered coolness and the upper wavy boundary provided constant heating. On fluid motion as well as energy transport, the impacts of Reynolds number, undulations number, and amplitude were examined. With a ripples number, significant energy carrier condensation was seen. In a conical diffuser, the study investigated turbulent flow of single and hybrid nanofluids [44]. It examined pressure losses and heat transfer at different Reynolds numbers and volume fractions of nanoparticles. Three forms of nanofluids, Al_2O_3, NEPCM_Al_2O_3, and nano encapsulated phase change material (NEPCM), were employed. The introduction of hybrid nanofluids made of nanoparticles, including and excluding phase change material (PCM), was a novel approach. The study found that the NEPCM nanofluid exhibited the most improved heat transmission and the least amount of pressure loss. It showed 15%, 10%, and 6% higher Nusselt numbers for NEPCM, NEPCM_Al_2O_3, and Al_2O_3, respectively. In comparison to the base fluid, there was a greater pressure drop, with a rise of 1% for NEPCM, 3.5% for Al_2O_3, and 5% for NEPCM_Al_2O_3 nanofluid. A review article also can be visited in order to understand the service of turbulent flow in order to understand the heat transfer in a rectangular enclosure [45].

Research Gap and Relevance with Recent studies: Our study investigates turbulent forced convection of hybrid nanofluids in an L-shaped channel, utilizing a comprehensive approach with multiple nanoparticle volume fractions and Reynolds numbers. Compared to previous studies, such as [46], which focus on thermal conductivity models and their Global Performance Index scores, our work provides detailed simulations on forced convection under specific flow conditions. Studies like [47] and [48] explore mixed and natural convection with different hybrid nanofluids, revealing significant heat transfer enhancements with nanoparticle volume fraction and fluid type, similar to our findings. Additionally, our work expands on [49], which examines heat transfer in steady laminar natural convection, by addressing more complex turbulent conditions and validating results using regression models. Our study's use of Reynolds numbers and nanoparticle combinations offers a deeper understanding of convection behaviors, complementing the results of these earlier investigations with practical application insights.

In this study, we investigate forced convection in an L-shaped channel using a hybrid nanofluid mixture of aluminum oxide and copper. The focus is on analyzing convection at the channel's inlet with Reynolds numbers ranging from 10,000 to 40,000. A numerical simulation is performed using COMSOL 5.6, applying Galerkin's Finite Element Method (FEM) to solve the governing equations, including the Navier-Stokes equation and the three-dimensional energy equation. The study examines various volume fractions (1% to 10%) of the hybrid nanofluid in a water-based fluid. We begin with a mesh independence study to evaluate parameters such as average velocity, average temperature, and Nusselt number. The numerical results are validated against established correlations for local Nusselt number and experimental data. The main objective is to explore the effects of volume fraction and Reynolds number on heat transfer, focusing on the minimum temperature at the channel edges, the local Nusselt number along the channel, and the relationship between Darcy friction factor and temperature. To perform the most suitable post-processing, a multiple linear regression procedure will be used to develop the regression equation related to the Reynolds number, copper volume fraction, and aluminum oxide volume fraction. Finally, researchers will compute absolute errors by comparing the numerical results with the predictions from the regression equations.

Application of finding: The findings discussed in this research examine fluid flow and heat transfer through the use of hybrid nanofluids composed of copper and aluminum oxide, which have extensive applications in advanced cooling and thermal management systems. The temperature behavior within the L-shaped domain, along with the enhanced heat transfer rate achieved by increasing the Reynolds number and the nanoparticle volume fraction, can be applied in electronic cooling, efficient heat exchangers, and energy systems, where effective heat dissipation is critical. Our derived regression equations for average outlet temperature and Nusselt number provide a practical tool for engineers to design systems with specific heat transfer and flow conditions. This article offers a detailed analysis of thermal and flow patterns in nanofluid channels, contributing valuable insights for the expanding applications of nanofluids in engineering fields.

MATERIALS AND METHODS

The schematic diagram of the L-shaped channel is depicted in Fig. 1, which will be examined in the current article for its heat transfer characteristics via the conventional process involving the hybrid mixture. The transportation of the hybrid mixture comprises copper and aluminum oxides as nanoparticles in a water-based fluid. The three-dimensional geometry is structured with a horizontal and vertical block joined together, maintaining a constant channel length for these blocks. In the block along the x-axis the width L_y = 50% L_x and the length along the z-axis L_z =10% L_x, while in a vertical block, the thickness L_y = 10% L_x and width L_z = 50% L_x. In this physical geometry, the area is identified as the channel inlet, where the nano-mixture is introduced with an x-velocity. Zero-pressure conditions and backflow are controlled at the end of the channel. Aside from these two boundaries, all other boundaries function as no-slip walls.

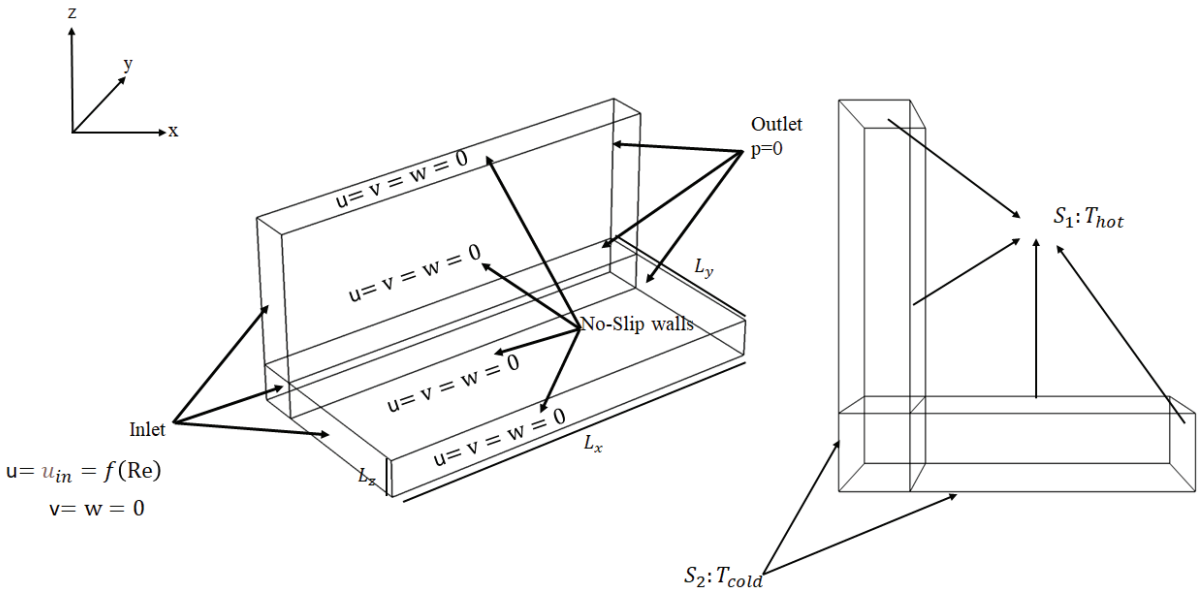

Figure 1. The schematic looks at the three-dimensional L-shaped channel with boundary conditions.

To examine the distribution of heat energy along the selected channel, we plan to divide the channel into two sections, denoted as S_1 and S_2, where hot and cold temperatures will be imposed, respectively, as shown in Figure 1. The hybrid mixture of copper (Cu) and aluminum oxide (Al_2O_3) will flow through the base fluid with volume fractions of 1%, 4%, 7%, and 10%. In order to assess the impact of forced convection through the L-shaped channel, Reynolds numbers ranging from 10,000 to 40,000 are utilized. We employ COMSOL Multiphysics 5.6, a finite element-based software, to create a numerical simulation of this problem, incorporating the turbulence and energy equations in three dimensions. Table 1 provides a detailed overview of the thermo-physical properties of the nanofluid and other parameters used in this study.

Table 1. Thermo-physical characteristics of the hybrid mixture and other parameters used in simulation [50-52]

Explanation	Symbol	Value
The volume fraction of Al_2O_3	ϕ_1	0.01, 0.04, 0.07, 0.1
The volume fraction of Cu	ϕ_2	0.01, 0.04, 0.07, 0.1
Density of Al_2O_3	ρ_1	3880 [kg/m^3]
Density of copper	ρ_2	8954 [kg/m^3]
The total density of the nanoparticles	ρ	$\frac{(\phi_1\rho_{np1}+\phi_2\rho_{np2})}{\phi_1+\phi_2}$
Specific heat of Al_2O_3	$(c_p)_1$	765 [J/kgK]
Specific heat of Cu	$(c_p)_2$	383.1 [J/kgK]
Specific heat of nanoparticles	c_p	$\frac{\phi_1\rho_{np1}(c_p)_{np1}+\phi_2\rho_{np2}(c_p)_{np2}}{\varphi\rho_{np}}$
The total volume fraction of nanoparticles	ϕ	$\phi_1+\phi_2$
Thermal conductivity of Al_2O_3	κ_1	40 [W/mK]
Thermal conductivity of Cu	κ_2	386 [W/mK]
Total thermal conductivity of the hybrid mixture	κ	$\frac{\phi_1\kappa_{np1}+\phi_2\kappa_{np2}}{\phi_1+\phi_2}$

Table 1. Thermo-physical characteristics of the hybrid mixture and other parameters used in simulation [50-52] (continued)

Explanation	Symbol	Value
The density of the water	ρ_{bf}	998 [kg/m^3]
Density of nanofluid	ρ_{nf}	$\rho_{bf}(1-\phi)+\phi\rho_{np}$
Specific heat of water	$(c_p)_{bf}$	4182 [J/kgK]
Specific heat of the hybrid mixture	$(c_p)_{nf}$	$\frac{\rho_{bf}(1-\phi)(\mathrm{c_p})_{bf}+\rho_{np}(1-\phi)(\mathrm{c_p})_{np}}{\rho_{nf}}$
Thermal conductivity of the water	κ_{bf}	0.597 [W/mK]
Thermal conductivity of the hybrid mixture	κ_{nf}	$\kappa_{bf}\left(\frac{\kappa_{np}+2\kappa_{bf}+2(\kappa_{np}-\kappa_{bf})\phi}{\kappa_{np}+2\kappa_{bf}-(\kappa_{np}-\kappa_{bf})\phi}\right)$
Water viscosity	μ_{bf}	0.000998 [Pas]
Nanofluid's viscosity	μ_{nf}	$\frac{\mu_{bf}}{(1-\phi)^{2.5}}$ [Pas]
Hydraulic diameter	d_h	4A/P
Reynolds number	Re	10,000-40,000
Inlet velocity	u_{in}	$\frac{\mu_{nf}\,\mathrm{Re}}{\rho_{nf}D_h}$
Cold temp	T_{cold}	293.15 [K]
Hot temp	T_{hot}	323.15[K]
Area of the total surface	Ar	$4(L_xL_z+L_yL_z+L_xL_y)-(\mathrm{L}_z)^2$
The perimeter of the channel	$\mathrm{P_e}$	$8L_x+8L_y+4L_z$
Velocity field	U	U=<u, v, w>
Temperature	T	
Turbulence kinetic energy	κ	
Turbulence dissipation rate	ε	

GOVERNING EQUATIONS AND $\kappa-\varepsilon$ TURBULENCE MODEL

In this model, the velocity field vector is denoted by U, which is further characterized by the velocity components u, v, and w, each possessing well-defined, continuous first-order partial derivatives. The context involves the modeling and simulation of heat transfer phenomena, specifically the flow of high-Reynolds-number hybrid nanofluids. In this scenario, it is prudent to adopt the $\kappa-\varepsilon$ model for investigation. This model proves to be an optimal choice due to its incorporation of both Turbulence kinetic energy and Turbulence dissipation rate considerations. Furthermore, the simulation encompasses a closed-channel geometry, such as an L-shaped channel, necessitating the selection of either a steady-state or time-independent study. These assumptions guide us in formulating the relevant equations, which are outlined below and also cited in [50-52].

Continuity Equation:

$$\rho_{nf}(\nabla\bullet\mathrm{U})=0 \tag{1}$$

Momentum Equation:

$$\rho_{nf}(\mathrm{U}\bullet\mathrm{U})\,\mathrm{U}-\nabla\bullet[-pI+(\mu_{nf}+\mu_T)(\nabla\mathrm{U}+(\nabla\mathrm{U})^t]=0 \tag{2}$$

$\kappa-\varepsilon$ Turbulence Model:

$$\rho_{nf}(\mathrm{U}\bullet\nabla)\kappa-\nabla\bullet\left[(\mu+\frac{\mu_T}{\sigma_\kappa})\nabla\mathrm{U}\right]-p_\kappa+\rho_{nf}\varepsilon=0 \tag{3}$$

$$\rho_{nf}(\mathrm{U}\bullet\nabla)\varepsilon-\nabla\bullet\left[(\mu+\frac{\mu_T}{\sigma_\kappa})\nabla\varepsilon\right]-c_{\varepsilon1}\frac{\varepsilon}{\kappa}+c_{\varepsilon2}\rho_{nf}\frac{\varepsilon^2}{\kappa}=0 \tag{4}$$

$$\text{Where } \mu_T = \rho_{nf} c_\mu \frac{\kappa^2}{\varepsilon} \text{ and } p_\kappa = \mu_T \left[\nabla \mathrm{U} : (\nabla \mathrm{U} + (\nabla \mathrm{U})^t\right] \quad (5)$$

$$\rho_{nf} (c_p)_{nf} \mathrm{U} \bullet \nabla T = \kappa_{nf} \nabla^2 T \quad (6)$$

Details of Physics On Boundaries Of L-Shaped Channel:

$$\textbf{Inlet: } u = u_{in} = f(\mathrm{Re}),\ \mathrm{v}=0,\ \mathrm{z}=0,$$
$$\kappa_0 = \frac{3}{2}(\mathrm{u}_{in} I_T)^2,\ \varepsilon_0 = \mathrm{c}_\mu^{3/2} \frac{\kappa_0^{3/2}}{L_T},\ \frac{\partial \mathrm{T}}{\partial n} = 0 \quad (7)$$

$$\textbf{Outlet: } \mathrm{x}=\mathrm{L}_x,\ 0 \le y \le L_y,\ 0 \le z \le L_z,$$
$$\frac{\partial \mathrm{T}}{\partial n} = 0 :\ \mathrm{p}_{out}=0,\ \nabla \varepsilon \bullet \mathbf{n} = 0 \text{ and } \nabla \kappa \bullet \mathbf{n} = 0 \quad (8)$$

$$\textbf{Along } S_1 :\ u = v = w = 0\ T = T_h, \text{ and}$$
$$\nabla \kappa \bullet \mathbf{n} = 0,\ \varepsilon = \rho_{nf} \frac{c_\mu \kappa^2}{\kappa_v \delta_w^+ \mu_{nf}} \quad (9)$$

$$\textbf{Along } S_2 \textbf{:}\ \mathrm{u} = \mathrm{v} = \mathrm{w} = 0,\ \nabla \kappa \bullet \mathbf{n} = 0$$
$$\text{and } \nabla \varepsilon \bullet \mathbf{n} = 0 \text{ and } \mathrm{T} = \mathrm{T}_c, \quad (10)$$

Here n is a vector perpendicular to the selected surface.

Turbulence intensity = I_T = 0.05, Turbulence length scale = L_T = 0.0126, δ_w^+ = 11.06.

Turbulence Variable [42]

κ_v	σ_κ	σ_ε	c_μ	$c_{\varepsilon 1}$	$c_{\varepsilon 2}$
0.41	1	1.3	0.09	1.44	1.92

It should be noted that the chosen ranges for turbulence kinetic energy and dissipation rates are compatible with the requirements for turbulence modeling in COMSOL Multiphysics. These values were carefully selected to ensure stable functioning of the turbulence model, enabling accurate computation of velocity and thermal profiles. This stability is essential to produce physically meaningful results that reflect the realistic behavior of hybrid nanofluid velocities [53].

Modeling Assumptions:

To model this phenomenon through the three-dimensional L-shaped channel the following assumptions will be made

1. The fluid flow is compressible, non-Newtonian and the time independent
2. The surface of the three-dimensional L-shaped channel is smooth no roughness was assumed along the upper or lower surface of channel
3. No back flow was assumed at the outelt of the channel
4. The initial values of the turbulent kinetic energy and the turbulence dissipation are enough to induce the turbulent in the channel.
5. The assumption ignores the dynamic interactions between nanoparticles and the fluid (e.g., Brownian motion, thermophoresis, or particle-fluid drag forces) and instead assumes the nanofluid behaves like a single-phase fluid.
6. Nanoparticles are assumed to be uniformly distributed at all points within the fluid. This neglects any possible local variations in concentration, which can occur in reality due to effects like sedimentation or particle clustering.
7. To drive the regression equations for the average temperature and the Nusselt number it is assumed that these variables are in a linear relationship with the Reynolds number, both volume fractions of the copper and alumina nanoparticles.
8. It is also assumed that we have sufficient data to form the linear regression equations.

Computational Parameters

- Prandtl Number: $\mathrm{Pr} = \frac{\mu_{nf} (c_p)_{nf}}{\kappa_{nf}}$ (11)
- Heat flux along the ith direction:
$$Q_i = \frac{\kappa_{nf}}{\kappa_{bf}} \frac{\partial T}{\partial i} \text{ where i=x, y and z} \quad (12)$$
- Heat transfer coefficient: $h_i = \frac{Q_i}{A(T - T_b)}$ (13)
- Bulk Temperature: $T_b = \frac{\iint_\Omega uT\ d\Omega}{\iint_\Omega \mathrm{u}\ d\Omega}$ (14)
- Local Nusselt number: $Nu_i = \frac{h\ \mathrm{i}}{k_{nf}}$ (15)
- Average Nusselt number:
- $(Nu_i)_{avg} = \frac{1}{A} \int_\Omega Nu_i\ dA$ Where A is the area of the selected boundary. (16)
- Darcy Friction Factor: $f_D = \frac{\tau_\omega}{\frac{1}{2} \rho_{nf} U_{mean}^2}$ (17)

Comsol Working Wagon Wheel

The software COMSOL flow algorithm is given below with the step-by-step procedure see Figure 2.

Overview of Methods For Non-Linear Pdes

For many decades, the question of how to solve nonlinear partial differential equations (PDEs) related to real-life applications and phenomena has been a significant challenge. Without timely solutions, controlling such phenomena becomes nearly impossible, often requiring substantial

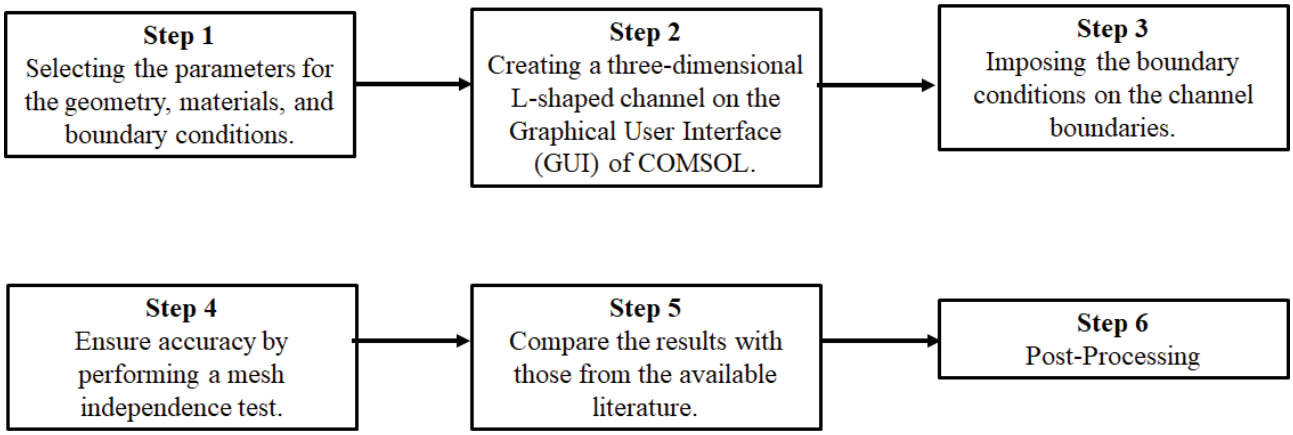

Figure 2. COMSOL Working Algorithm [53].

effort and continuous economic resources. Fortunately, numerical methods for solving PDEs provide approximate results promptly, allowing for practical applications in real-world scenarios. Various numerical schemes are now available to solve both individual nonlinear PDEs and systems of nonlinear PDEs. Some of these methods, along with their advantages and disadvantages, are summarized in the following table.

Table 2. A short description of the numerical schemes that solve the non-linear PDEs

Method	Description	Advantage	Disadvantage
Finite Difference Method (FDM)	Approximates derivatives by using finite differences between points, converting PDEs into algebraic equations. Requires iterative schemes for nonlinearity.	- Simple to implement, especially for structured grids. - Effective for time-dependent PDEs.	- Accumulated errors on coarse grids. - Challenging for complex boundaries and irregular domains.
Finite Element Method (FEM)	Divides the domain into subdomains (elements) and applies variational formulation, with iterative solvers for nonlinearity in each element.	- Highly accurate for complex geometries and variable material properties. - Flexible for various domains.	- Computationally intensive due to matrix assembly and inversion. - Requires expertise in meshing.
Finite Volume Method (FVM)	Integrates PDEs over discrete control volumes to ensure conservation laws are maintained, with algebraic transformation of nonlinear terms.	- Ideal for conservation laws (e.g., fluid dynamics). - Flux conservation across control volumes.	- Complex handling of boundary conditions, especially for unstructured grids. - Accuracy varies with grid type.
Multigrid Method	Solves nonlinear PDEs on hierarchical grids with relaxation steps at each level, accelerating convergence in large-scale problems.	- Highly efficient for large systems by reducing computational burden. - Fast convergence through multiple scales.	- Complex implementation requiring fine-tuning. - Performance depends on grid structure and relaxation techniques.

Multiple Linear Regression Procedure

Let n (64 in this case) be the size of the total population or the size of the dataset, and let k (3 in this case) be the number of total independent variables for which we are interested in writing the linear regression equation for a variable of interest. Let Y be the column vector which denotes the exact values of the dependent variable, and let $\hat{Y}$ also be the column vector denoting the predicted values of the dependent variables through the correlation process. The sizes of both Y and $\hat{Y}$ are $n\times1$ (64×1 in this case). Let X be the matrix, considering the size of $n\times(k+1)$ (64×4 in this case), which will have the values of the independent variables as the entries. Moreover, let B and E be the coefficient vector and the residual vector, which will have the sizes of $n\times1$ (64×1 in this case) and $n\times(k+1)$ (64×4 in this case), respectively.

These all matrices defined as above can be written as follow:

$$Y=[Y_1 \;\; Y_2 \;\; Y_3 \;\; \ldots \;\; Y_n]^T,\; \hat{Y}=[\hat{Y}_1 \;\; \hat{Y}_2 \;\; \hat{Y}_3 \;\; \ldots \;\; \hat{Y}_n]^T,$$

$$B=[b_0 \;\; b_1 \;\; b_2 \;\; \ldots \;\; b_k]^T$$

$$E=[\varepsilon_1 \;\; \varepsilon_2 \;\; \varepsilon_3 \;\; \ldots \;\; \varepsilon_n]^T \text{ and}$$

$$X=\begin{bmatrix} 1 & X_{11} & X_{12} & \ldots & X_{1k} \\ 1 & X_{21} & X_{22} & \ldots & X_{2k} \\ .. & .. & .. & .. & .. \\ 1 & X_{n1} & X_{n2} & \ldots & X_{nk} \end{bmatrix} \tag{18}$$

Considering the above all matrices, we can write a system in the matrix form as **Y = XB + E** where **X** is the matrix of independent k variable and this system can be written in equivalent form as:

$$\mathbf{Y}=b_0+b_1\mathbf{X_1}+b_2\mathbf{X_2}+\ldots+b_k\mathbf{X_K}+\varepsilon \tag{19}$$

Initially, the matrix Y and the matrix X of the values are given and then B, Y' and E will be computed as $B=(X^TX)^{-1}X^TY,\; \hat{Y}=\mathbf{X}B$ and $E=Y-\hat{Y}$.

After computing the all above values the following ANOVA (Analysis Of Variance) table will be made.

	Degree of Freedom (Df)	Sum of Squares (SS)	Mean of the Squares (MF)	F-Statistic
Regression	DFR=k	$SSR=\sum_1^n(\hat{Y}-Y_{mean})^2$	$MSR=\frac{SSR}{DFR}$	$F=\frac{MSR}{MSE}$
Residual	DFE=n-k-1	$SSE=\sum_1^n(Y_i-\hat{Y}_i)^2$	$MSE=\frac{SSE}{DFE}$	
Total	n-1	$SSE=\sum_1^n(Y_i-Y_{mean})^2$		

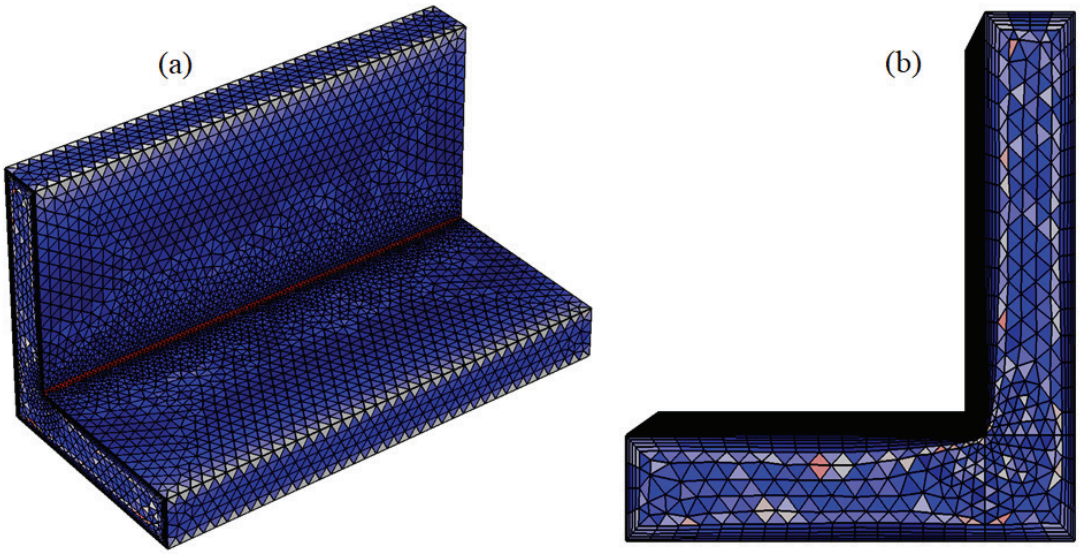

Figure 3 (a-b). The schematic diagram for the meshing procedure of the L-shaped channel.

Table 3. Final meshing construction information

Information	Number of elements
Mesh vertices	47,217
Tetrahedra	1,35,954
Pyramids	1080
Prisms	42,490
Triangles	10,238
Quads	804
Number of elements at the edges of the channel	590
Number of elements of vertices	16
Minimum quality of the element	0.01484
Average qualities	0.5616
Element volume ratio	0.003468
Mesh volume	0.09 cm^3
Total number of elements	1,80,729

After finding the F value a critical value will be searched F_a by using the F-Distribution Table that corresponds to the value (DFR, DFE) to decide the one of the hypothesis.

$$\begin{aligned} H_0 &: b_i = 0 \quad \text{if } F<F_\alpha \text{ (Failure)} \\ H_1 &: b_i \neq 0 \quad \text{if } F>F_\alpha \text{ (Success)} \end{aligned} \tag{20}$$

Where $\alpha = 0.05$ is the significance level. The above procedure is referenced in [54-56]

Mesh Independent/Grid Independence Test and Validation with Literature

In numerical simulations like finite element analysis, achieving a high level of accuracy often requires an assessment of how mesh density influences the results, commonly referred to as a "mesh independence" or "grid independence" test. For the present study, an L-shaped channel is modeled to simulate the flow of a hybrid nanofluid mixture of aluminum oxide (Al_2O_3) and copper (Cu) in water. The aim of the mesh independence study is to ensure that numerical results for average velocity, average temperature, and average Nusselt number are accurate and not significantly affected by further refinement of the mesh. The mesh consists of multiple element types, including tetrahedral, prism, triangular, and quadrilateral elements, which provide flexibility and ensure a robust representation of the geometry. The mesh refinement process systematically increases the number of elements to observe changes in key parameters. In Fig. 4 (a-c), the X-axis represents the total number of elements used in the simulation, while the Y-axis displays the computed values for average velocity, average temperature, and average Nusselt number. Each parameter stabilizes and converges to a nearly constant value when the number of elements reaches approximately 150,000, indicating that further increases in mesh density have negligible effects. This convergence confirms that 150,000 elements achieve mesh independence for this model. However, to ensure the highest accuracy, the final simulation uses a mesh with 180,729 elements, providing additional refinement beyond the convergence threshold. A complete structure of the mesh system can be seen in Table 3.

After completing the mesh independence study, we will validate the computational results in this study by comparing them to the correlations available in references [50] and [51]. To achieve this, we calculate the local Nusselt number as a function of temperature using the two correlations (21) and (22) and apply the basic formula for the local Nusselt number, as depicted in Fig. 5. It is evident that the current methodology for obtaining numerical results aligns well with these correlations, and the numerical simulations conducted using this software are expected to achieve an accuracy of approximately 98%.

$$\text{Dittus and Boelter: } Nu_x = 0.023\,\mathrm{Re}^{0.8}\,\mathrm{Pr}^{0.4} \tag{21}$$

$$\text{Dawid and Jan: } \mathrm{Nu}_x = 0.02155\mathrm{Re}^{0.8018}\mathrm{Pr}^{0.7095} \tag{22}$$

We have performed comparative validation with an experimental study, which reinforces our findings through a correlation with the Dittus-Boelter equation [50]. The experimental study utilized a reverse L-shaped channel to enhance thermal performance, benchmarking the experimentally obtained Nusselt number against the Dittus-Boelter correlation. This experimental work [56] also employed the $\kappa - \varepsilon$ turbulence model, consistent with the model applied in our investigation. By using this model to analyze heat transfer characteristics in an L-shaped channel, we ensure alignment with established methodologies. As illustrated in Figure 6, our numerical results show strong agreement with the experimental data, affirming the robustness of our approach and the validity of the outcomes.

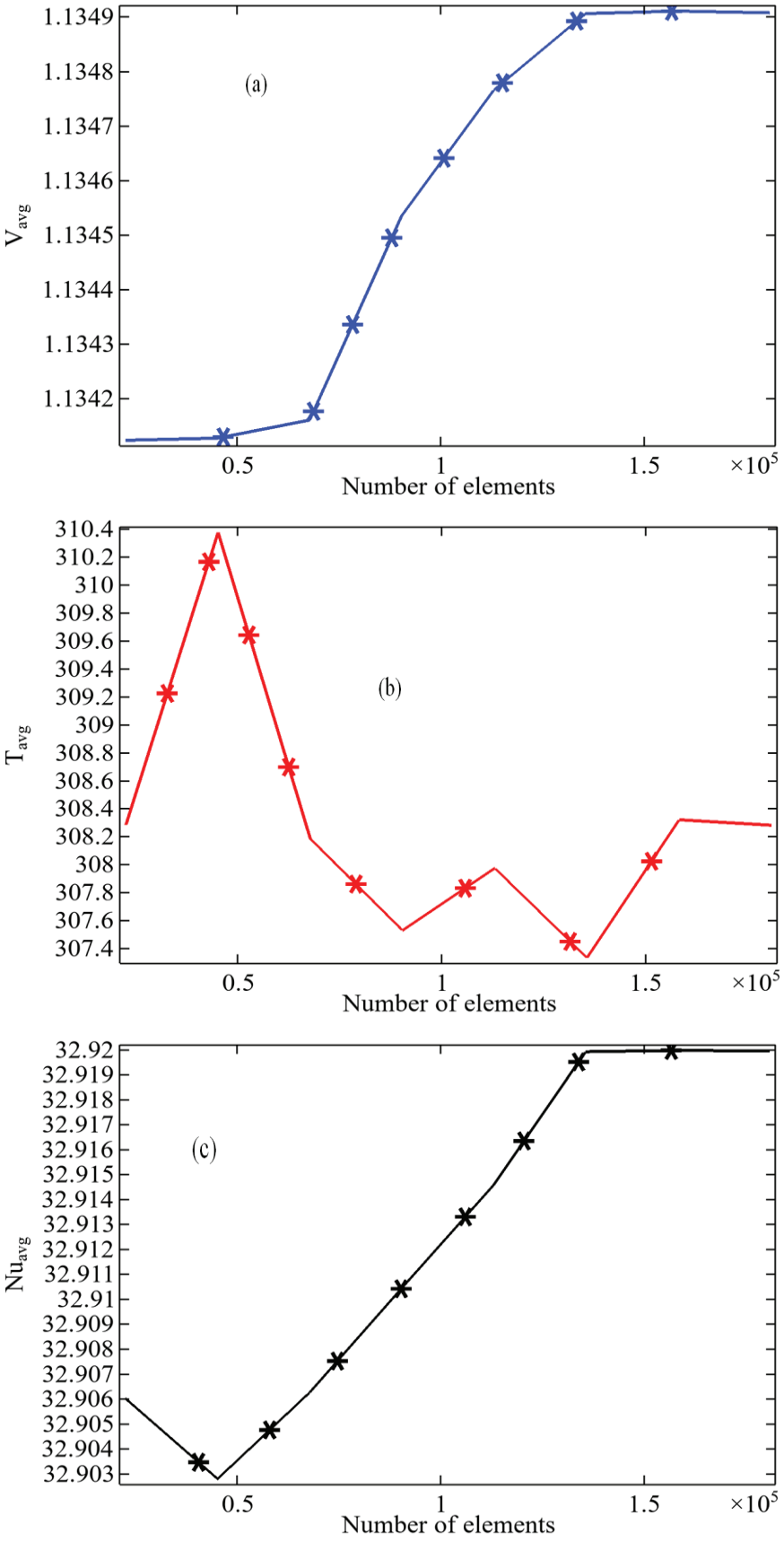

Figure 4(a-c). For the mesh-independent or grid-independent study (a) V_{avg}, (b) T_{avg}, and (c) Nu_{avg} have been calculated.

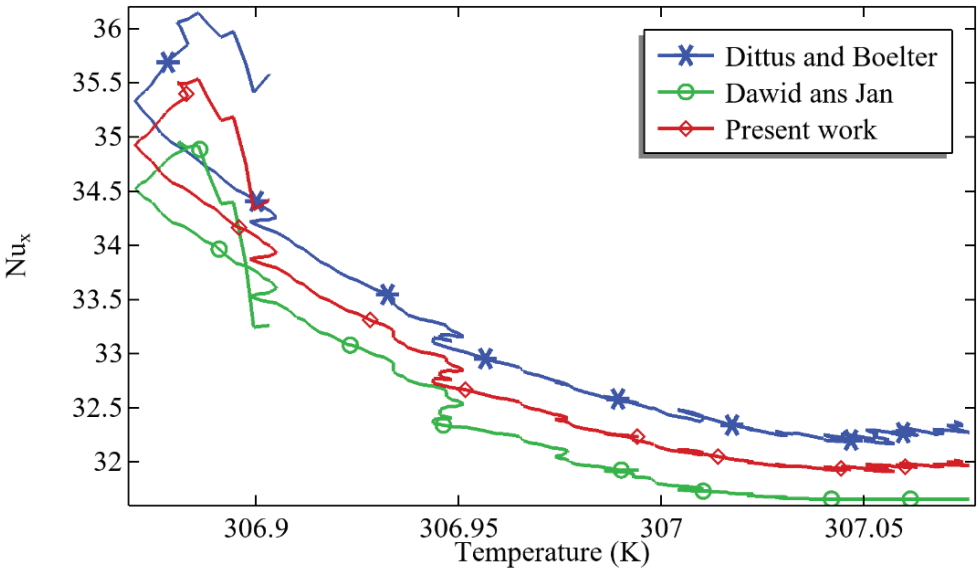

Figure 5. The evaluation of Nu_x against the temperature along the x-axis by using correlations and the present work at $\phi_1 = \phi_2 = 1\%$.

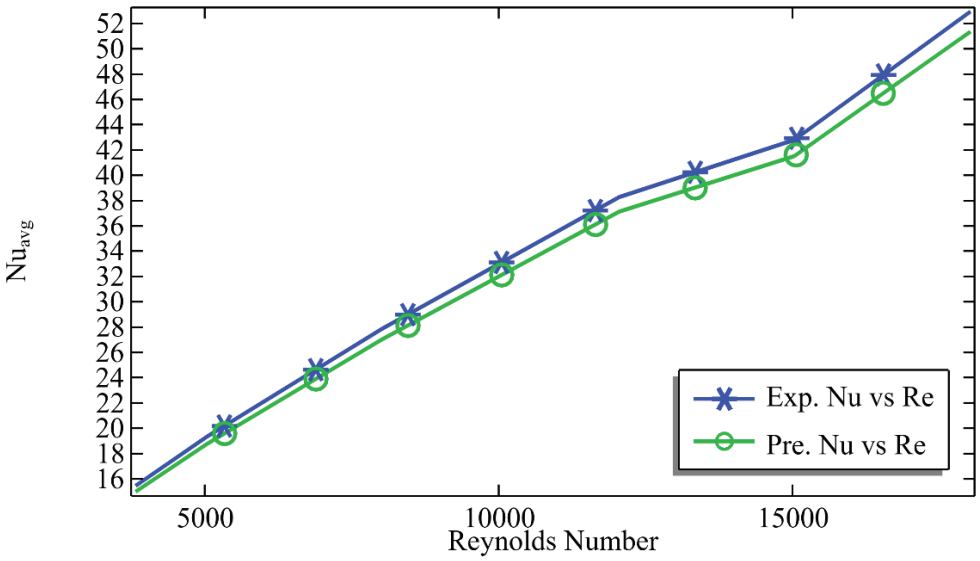

Figure 6. Comparison of the average Nusselt number versus Reynolds number between the present study and previous studies.

RESULTS AND DISCUSSION

In the current article, a numerical investigation of a three-dimensional L-shaped channel is conducted, employing hybrid nanofluids in the context of transport applications. The study utilizes the three-dimensional incompressible Reynolds-averaged Navier-Stokes equations and three-dimensional heat equations to analyze fluid dynamics and energy distribution within the channel. Copper and alumina nanoparticles, assumed to be spherical, are suspended in water as base fluids. The simulation, carried out using COMSOL Multiphysics 5.6 and finite element method, successfully explores turbulent forced convection under varying Reynolds numbers (10,000 to 40,000) and nanoparticle concentrations (0.01-0.1). This research aims to contribute to the control of minimum temperature, local Nusselt number (a ratio of convection to conduction processes), and Darcy friction factor vs the temperature by altering parameters. While this study is relatively rare in the fluid dynamics field, it holds significant applications due to the vertical separation of flow along the junction.

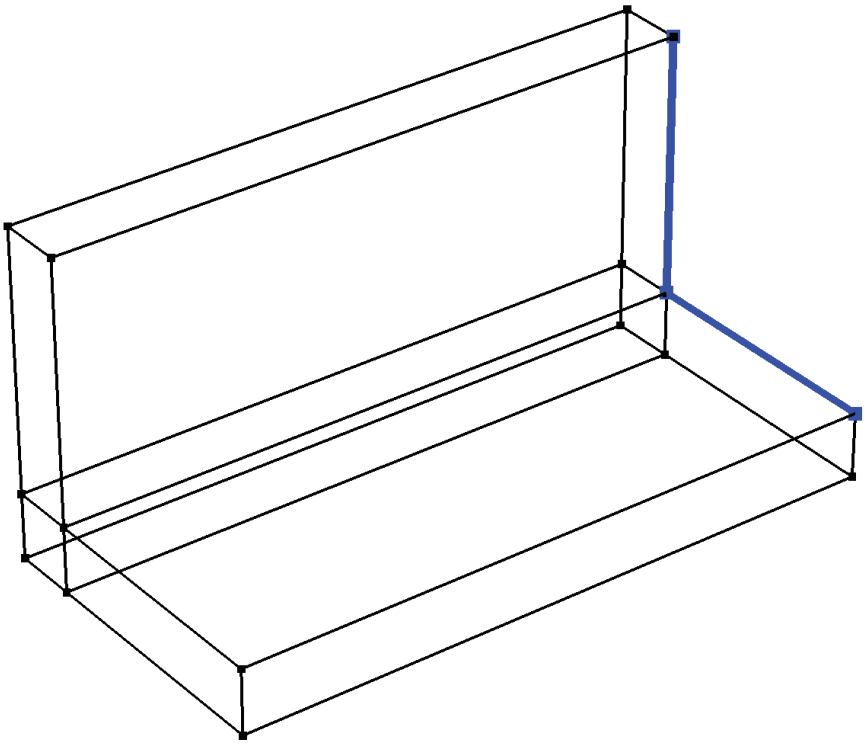

Figure 7. Edges pic for minimum temperature.

Minimum Temperature and Linear of Average Temparature

In Figure 7, a schematic diagram of a three-dimensional L-shaped structure is shown, with two edges depicted at the end. Our main objective is to discuss the minimum temperature at this section while altering two out of three parameters. We are focusing on the behavior of the minimum temperature at these two edges. Finally, a general regression equation will be provided that can be used for future predictions or for verifying the present investigation. The methodology will involve multiple linear regression steps to generate empirical equations.

In Figure 8(a-d), the minimum temperature is plotted against the increasing volume fraction of alumina and the Reynolds number. For each curve shown in these figures, the Reynolds number is fixed, while the volume fraction of copper is fixed for all figures, indicating that these results are for hybrid nanofluids. In Figure 8(a), for fixed Reynolds numbers and a fixed volume fraction $\phi_2 = 0.01$), the minimum temperature decreases as the volume fraction of alumina increases from 0.01 to 0.04, and then it increases for all Reynolds numbers from 10,000 to 30,000. However, at a value of 40,000 for the Reynolds number, the minimum temperature begins to decline at $\phi_1 = 0.07$, indicating that there are two critical values of ϕ_1 where the behavior of the minimum temperature alters. In Figure 8(b), the minimum temperature is plotted against ϕ_1 while fixing the Reynolds number for all curves, and the volume fraction of copper (ϕ_2) is fixed at 0.04. Compared to Fig. 7(a), it can be observed that the minimum temperature always increases for all values of ϕ_1 at Re = 10,000, which is also an indication of the application of hybrid nanofluids in heat transfer rate improvement. In both Figs 8(a) and 8(b), it can be understood that increasing the Reynolds number increases the minimum temperature at the two edges of the three-dimensional L-shaped channel. In Figure. 7(b), it can be observed that using the two Reynolds numbers of Re = 30,000 and 40,000, the maximum minimum temperature is achieved at $\phi_1 = 0.1$.

In Figure 8(c) and Figure 8(d), the minimum temperature is analyzed against the increasing concentration of alumina in the base fluids, while the Reynolds number is fixed for each curve. We observe that in both figures, the minimum temperature increases with the enhancement of the Reynolds number for higher volume fractions of alumina. While the concentration of copper was fixed at 0.07 and 0.1 in both figures, we found that the minimum temperature at the end of these two edges depends on both the Reynolds number and the concentration of nanoparticles in the base fluids. However, from all these figures, it is very challenging to control the temperature at the two edges, and this depends on several factors, including the geometry. In Figure. 7(d), it can be easily understood that to achieve the minimum temperature for a high level of concentration of copper, the Reynolds number should be fixed at Re = 30,000.

To analyze the variation in minimum temperature patterns with increasing copper nanoparticle concentration

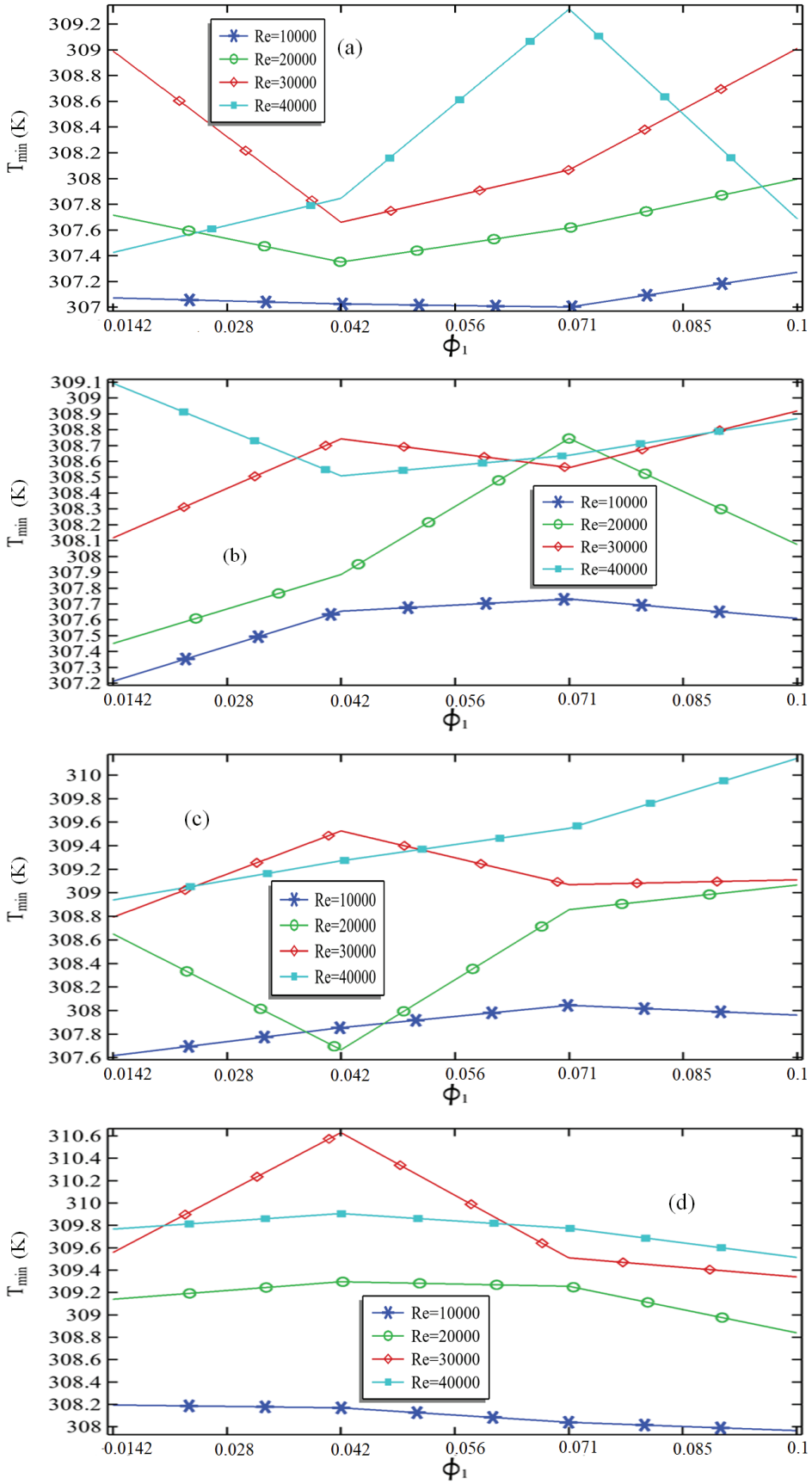

Figure 8(a-d). The minimum temperature at the two edges of the channel against ϕ_1 fixed Reynolds numbers (a) $\phi_2 = 0.01$ (b) $\phi_2 = 0.04$ (c) $\phi_2 = 0.07$ and (d) $\phi_2 = 0.1$.

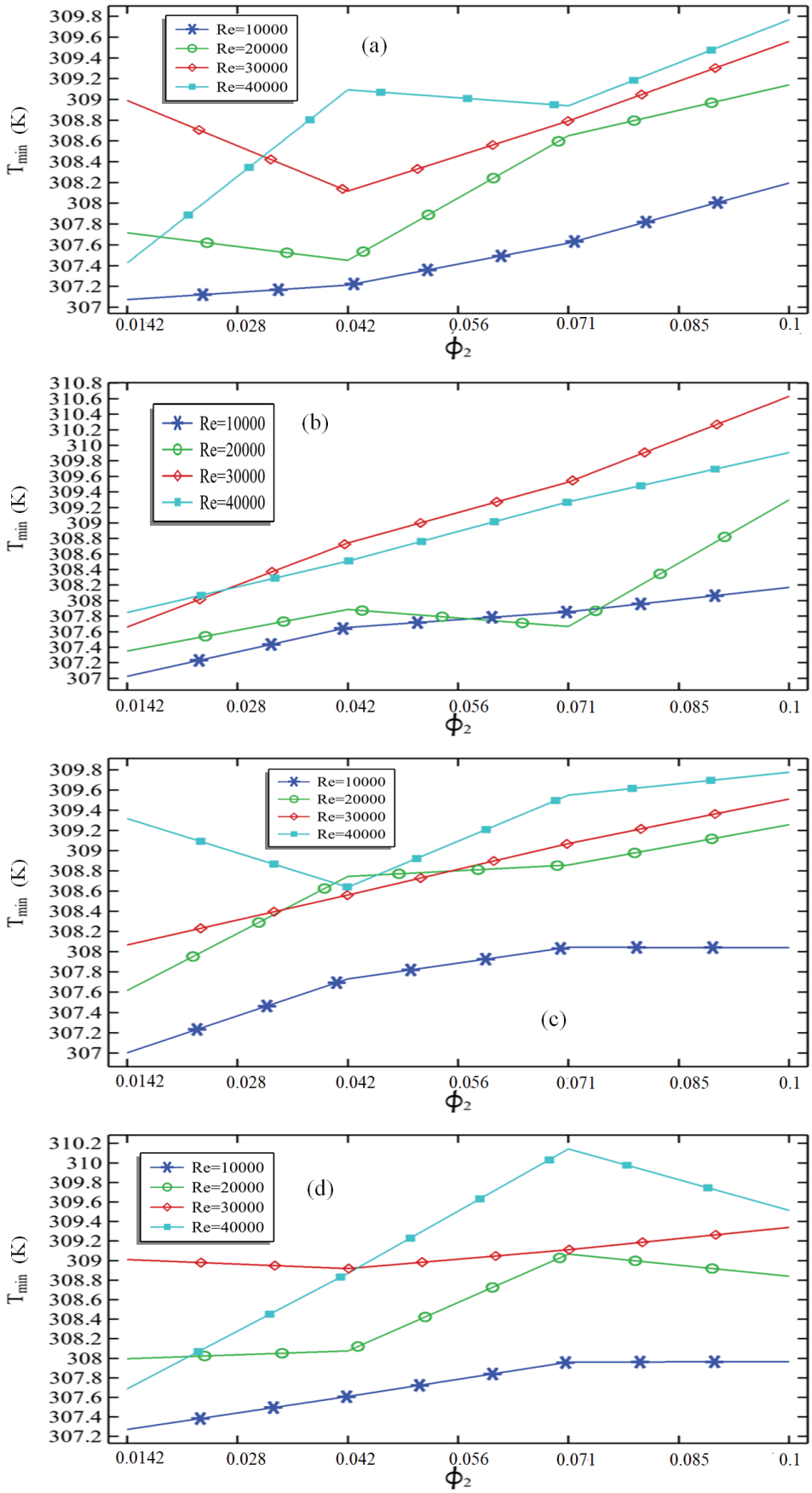

Figure 9(a-d). The minimum temperature at the two edges of the channel vs ϕ_2 for fixed Reynolds numbers at (a) $\phi_1 = 0.01$ (b) $\phi_1 = 0.04$ (c) $\phi_1 = 0.07$ and (d) $\phi_1 = 0.1$.

while keeping the Reynolds number constant, Figures 9(a-d) are presented. After each figure, the alumina concentration is progressively increased. In Figure 9(a), an evident increase in minimum temperature at the outlet edges is observed with higher copper volume fractions for each fixed Reynolds number. A comparison with Fig 9(a) reveals that utilizing copper leads to a more rapid temperature increase at the two edges. Notably, at the lowest Reynolds number, the minimum temperature remains elevated, displaying an irregular pattern for other Reynolds numbers. However, employing a copper volume fraction of 0.1 in the base fluids yields the highest minimum temperature for all Reynolds numbers due to copper's superior thermal conductivity compared to alumina nanoparticles.

In Figure 9(b), with the alumina volume fraction fixed at $\phi_1 = 0.04$ (compared to 0.01 in Figure 8(a)), an increasing alumina concentration correlates with a higher minimum temperature. This figure indicates that the maximum minimum temperature is attained at a Reynolds number of 30,000. Here, for most Reynolds numbers, the minimum temperature straightforwardly increases. In Figures 9(c) and 9(d), scrutinizing minimum temperature patterns by further increasing alumina nanoparticle concentration reveals a consistent increase across all Reynolds numbers compared to the previous results in Figures 9(a) and 9(b). Notably, only at Re = 10,000 does the minimum temperature increase without obstruction. Additionally, using $\phi_1 = 0.01$ and 0.04 of copper nanoparticles appears to be critical points, altering the pattern. For high Reynolds numbers and elevated copper nanoparticle concentrations, the minimum temperature at the two edges of the L-shaped channel increases, presenting an irregular pattern with increasing Reynolds number and volume fraction of copper and alumina nanoparticles. Overall, the successful outcome underscores that utilizing hybrid nanofluids consistently enhances heat transfer rates, as evident in the present results for the minimum temperature.

Physical reasons: The observed behavior is attributed to the physical properties of hybrid nanofluids and their interactions with flow dynamics within the domain. Copper's superior thermal conductivity enhances the heat transfer rate, leading to increased minimum temperatures at the edges of the L-shaped channel. At very high Reynolds numbers, intensified fluid velocity increases turbulent mixing, improving thermal energy distribution. The behavior at specific volume fractions occurs due to the balance between enhanced thermal conductivity and increased viscosity from the nanoparticle concentration, which can impede flow. Alumina's lower thermal conductivity compared to copper results in varying contributions to heat transfer. The geometry of the L-shaped channel influences recirculation zones, creating localized temperature variations at the channel edges. Additionally, the interplay between nanoparticle concentration and Reynolds number determines the extent of boundary layer disruption, affecting heat transfer rates at the edges.

After analyzing the numerical results for the minimum temperature in Figures. 9(a-d) and 9(a-d) by altering the parameters, it was found that the volume fraction of both nanomaterials exhibits an irregular pattern in depicting the minimum temperature. In other words, the minimum temperature in the L-shaped channel appears to be independent of the volume fraction of these nanomaterials in the base fluids. Therefore, based on these observations, we are drawing a conclusion through the linear regression procedure that will determine the average temperature at the outlet of the three-dimensional L-shaped channel using the multiple linear regression process, as given below:

$$T_{avg,Predicted} = 307.117188 + 0.0000132\,\mathrm{Re} \qquad (23)$$

According to this equation (23), the average temperature in this study depends purely on the Reynolds number in the case of turbulence investigation. The equation can also be used for future predictions when conducting similar studies. However, the utility of this equation depends on the parameters used, as it provides only an estimation of the average temperature at the outlet. Table 4 summarizes the top parameter estimators that can be used to minimize

Table 4. Top 10 minimum absolute errors when comparing the exact average temperature at the outlet with the temperature predicted by the linear regression

ϕ_1	ϕ_2	Re	$T_{avg,Exact}$	$T_{avg,Predicted}$	$\lvert T_{avg,Exact} - T_{avg,Predicted} \rvert$
0.01	0.1	40000	307.64	307.645188	0.005188
0.1	0.07	20000	307.39	307.381188	0.008812
0.04	0.07	10000	307.24	307.249188	0.009188
0.07	0.07	40000	307.66	307.645188	0.014812
0.04	0.1	20000	307.4	307.381188	0.018812
0.1	0.1	10000	307.27	307.249188	0.020812
0.01	0.07	10000	307.2	307.249188	0.049188
0.04	0.1	10000	307.3	307.249188	0.050812
0.07	0.1	10000	307.19	307.249188	0.059188
0.01	0.01	20000	307.32	307.381188	0.061188

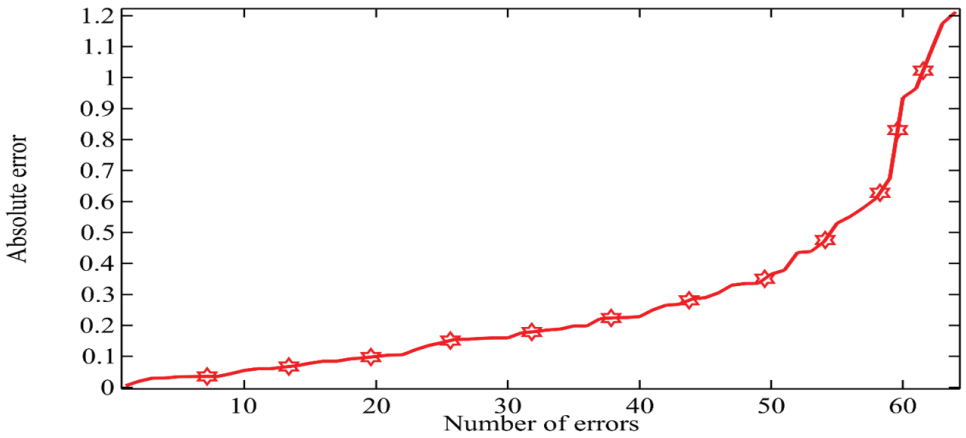

Figure 10. The graph of absolute error due to the comparison exact average temperature at the outelt and the average temperture through the correlation vs the number of errors.

absolute error in such studies. According to this table, when using $\phi_1 = 0.01$, $\phi_2 = 0.1$, and Re = 40,000, the absolute error due to the comparison of the exact average temperature and predicted average temperature is approximately 0.005528. The relation also defines that by increasing per unit of the Reynolds number the temperature rises by 0.0000132.

Finally, a graph is attached summarizing the absolute error when predicting the original temperature using linear regression equation. It should be noted that by utilizing different ranges of three parameters, we have conducted 64 simulations. Figure 10 suggests that approximately 30 numerical simulations yield a minimum absolute error of less than 0.2, while the maximum error that can be achieved when computing the average temperature via the linear regression equation is 1.2.

Local Nusselt Number and The Linear Regression Equation of Average Nusselt Number

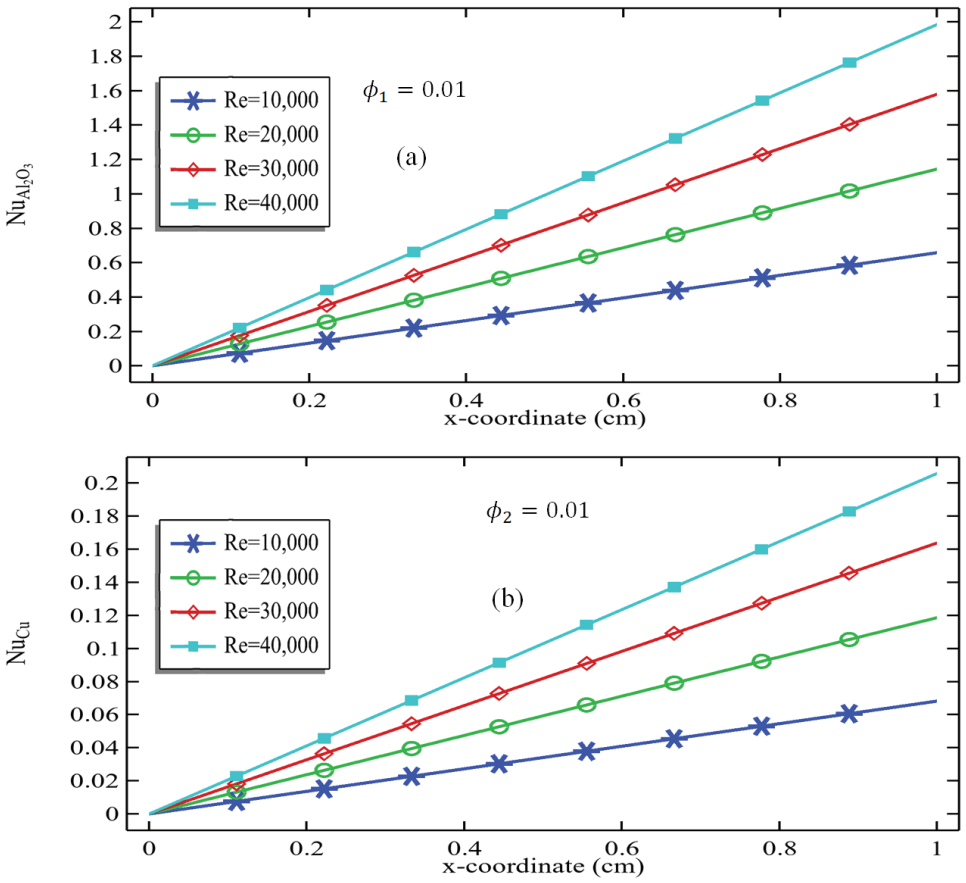

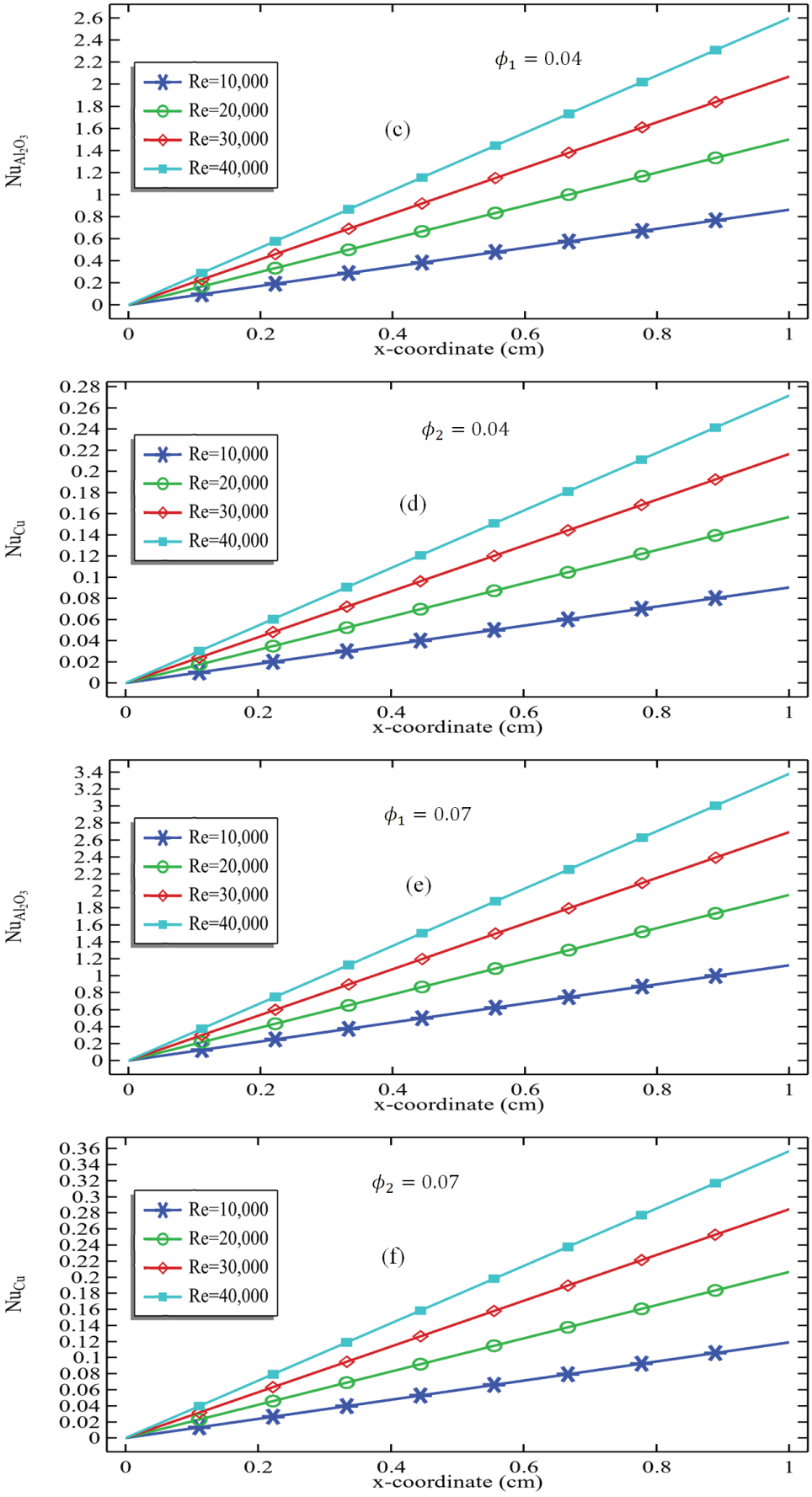

Figure 11(a-f). The computational results for the local Nusselt number along the channel's length for aluminum oxide and copper separately.

It is crucial to measure the effectiveness of both convection and conduction processes in a domain, which depends on the heat transfer coefficient and thermal conductivity, respectively. The local Nusselt number or average Nusselt number is often measured during numerical investigations, serving as a good indicator for both convection and conduction. An increase in the Nusselt number suggests stronger convection, while a decrease indicates stronger conduction. For heat transfer investigation and optimization, two different nanoparticles, copper, and alumina, are suspended in base fluids. The aim is to analyze which nanoparticle contributes more to the convection process. Figure 11(a-f) compares local Nusselt numbers along the x-axis, considering the same volume fraction of nanomaterials in base fluids. Figures 11 (a) and 11 (b) show volume fractions for both nanomaterials set at 0.01, revealing an increase in local Nusselt numbers for each fixed Reynolds number. The maximum local Nusselt at the end of the x-axis improves with higher Reynolds numbers, indicating a significant contribution of Reynolds number to convection enhancement. Comparatively, using alumina nanoparticles demonstrates a higher contribution to the enhancement of the convection process compared to copper nanomaterials. This is attributed to the stronger thermal conductivity of copper, which strengthens the conduction process. In Figures 11 (c) and 11 (d), with a volume fraction of 0.04, increasing the volume fraction of nanomaterials in base fluids enhances the local Nusselt number and convection process. Reynolds number also plays a crucial role in increasing convection, as seen in the measurement of the maximum local Nusselt number at the channel outlet with increasing Reynolds numbers. Figures 11 (e) and 11 (f) continue to confirm that higher volume fractions (0.07) of alumina and copper nanomaterials enhance the convection process along the x-axis. Alumina proves to be a superior nanoparticle for convection enhancement, and increasing Reynolds numbers further contribute to the local Nusselt number. In summary, using alumina nanoparticles is effective for increasing the convection process, while copper excels in conduction due to its thermal conductivity. Additionally, an increase in Reynolds numbers significantly contributes to convection rate enhancement in the domain. After observing that the local Nusselt function is purely related to the Reynolds number and the volume fractions of both alumina and copper nanomaterials, further analysis is warranted. Therefore, to draw more conclusive results, a multiple linear regression process described in section (2.2) will be applied to establish the linear regression equation between the Reynolds number and the volume fractions of both nanomaterials to yield or to predict the local Nusselt number at the outlet of the channel. The equation is described as follows:

$$\mathrm{Nu}_{\mathrm{Predicted}} = 11.642265 + 13.492917\phi_2 + 0.00224559\,\mathrm{Re} \quad (24)$$

Finally, Table 5 is attached, which describes the top 10 minimum absolute errors obtained by comparing the exact Nusselt number values at the outlet with the predicted Nusselt numbers from the correlation. From the table, it can be seen that the correlation works well when the volume fraction of both nanomaterials is kept at 0.01 and the Reynolds number is maintained at 30,000. The linear regression equation described above is only valid when investigating such a type of three-dimensional L-shaped channel using the $\kappa - \varepsilon$ turbulence model and analyzing the thermal properties of hybrid nanofluids. The equation above suggests that increasing each unit of copper volume fraction and Reynolds number results in the average Nusselt number at the outlet increasing by 13.492917 and 0.002245559, respectively.

Finally, a graph in Figure 12. is provided, where the absolute error (difference between exact and predicted average Nusselt numbers) is plotted against the total number of errors. Since multiple values of the parameters have been used, about 64 numerical simulations were conducted to analyze the heat transfer characteristics for the

Table 5. The top 10 minimum absolute errors when computing the difference between the exact average Nusselt number at the outlet and the predicted Nusselt number via correlation

ϕ_1	ϕ_2	Re	Nu_{Exact}	$Nu_{Predicted}$	$\lvert Nu_{Exact} - Nu_{Predicted} \rvert$
0.01	0.01	30000	79.513	79.14489417	0.36810583
0.01	0.04	30000	80.174	79.54968168	0.62431832
0.04	0.01	30000	79.801	79.14489417	0.65610583
0.1	0.01	10000	33.481	34.23309417	0.75209417
0.1	0.04	40000	101.23	102.0055817	0.77558168
0.1	0.1	30000	81.143	80.3592567	0.7837433
0.07	0.07	40000	101.62	102.4103692	0.79036919
0.04	0.1	40000	101.99	102.8151567	0.8251567
0.1	0.07	40000	101.58	102.4103692	0.83036919
0.07	0.01	10000	33.384	34.23309417	0.84909417

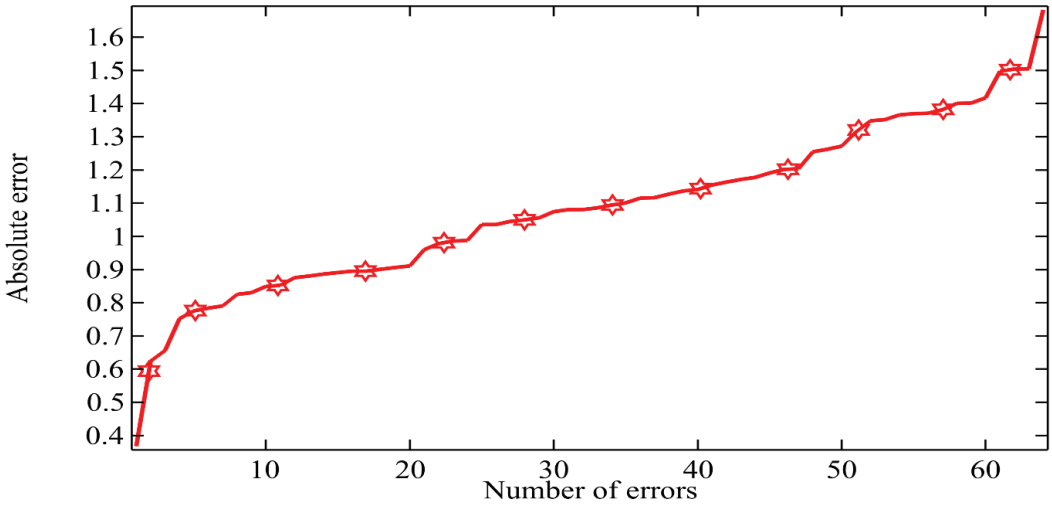

Figure 12. The graph of absolute error vs the number of errors.

three-dimensional L-shaped channel using turbulence modeling. The graph in Figure. 12. indicates that approximately 30 simulations yield an absolute error of 1.1 when comparing the exact average Nusselt number with the predicted Nusselt number. The maximum absolute error achievable using the correlation as the predictor is 1.6.

Calculation and Presentation of Darcy-Weisbach Friction Factor

In this section, the relationship between temperature and the friction factor, as described by the Darcy-Weisbach formula, is analyzed along the x-axis. The pattern is also examined using the Reynolds number and volume fraction of nanomaterials in the base fluids. Friction measures the fluid's resistance due to increased material density. Figures. 13(a-d) and 14(a-d) illustrate the pattern of friction factor vs temperature. In Figures. 13(a-d), the volume fraction of alumina varies for each curve, while the Reynolds number is fixed. In Figure. 13(a), with a fixed Re = 10,000, the friction factor increases with temperature, reaches a maximum, and then decreases for each alumina volume fraction. Interestingly, the Darcy friction factor remains constant for all alumina concentrations, showing a consistent pattern with increasing temperature. For $\phi_1 = 0.04$, Figure. 13(a) yields the maximum temperature with the same friction factor. In Figures. 13(b) and 13(c), Reynolds numbers of 20,000 and 30,000 are checked with increasing volume fraction of alumina. The friction factor vs temperature pattern remains the same as in Figure. 13(a), indicating an increase, peak, and decline. Additionally, an irregular pattern is observed with higher volume fractions in Figures. 13(b) and 13(c), reaching minimum and maximum temperatures at different phi values. Figure. 13(d) shows that the friction factor yields the maximum temperature in the L-shaped channel with $\phi_1 = 0.04$. However, across all figures, increasing Reynolds number consistently leads to a decline in maximum temperature due to higher velocity and momentum forces in the channel. It's noteworthy that increasing friction force reduces fluid density and mean flow velocity, allowing for better heat exchange with the surroundings.

In Figs 14(a-d), we investigate the relationship between the Darcy friction factor and temperature patterns by varying the volume fraction of copper and Reynolds number, with the alumina fraction fixed at 0.02. Notably, in Figure 14(a), an intriguing observation emerges: as the volume fraction of copper increases, the temperature exhibits variation for a constant friction factor. This phenomenon, akin to previous findings (cf. Figure. 13(a-d)), reveals a non-linear trend whereby an initial rise in temperature coincides with an increase in the Darcy friction factor, reaching a peak before declining. Emphasizing the pivotal role of temperature control via volume fraction manipulation, we underscore the complementary influence of Reynolds number modulation. Moving to Figure 14(b), where the Reynolds number is set at 20,000, we observe a noteworthy shift in the position of friction factor-temperature profiles with increasing volume fraction. Specifically, at constant friction factors, $\phi_2 = 0.1$ yields higher temperatures along the x-axis compared to $\phi_2 = 0.01$. To provide a comprehensive analysis, Figures 14(c) and 14(d) are introduced, fixing Reynolds numbers at 30,000 and 40,000, respectively. Herein, a decrease in the maximum Darcy friction factor is evident with increasing Reynolds number, attributed to heightened fluid velocities or flow rates, thereby reducing frictional effects.

Furthermore, an intriguing irregularity surfaces in the friction versus temperature graph due to volume fraction alterations, underscoring the nuanced interplay between these variables. It is noteworthy that achieving precise control over the friction factor-temperature relationship solely via copper volume fraction manipulation

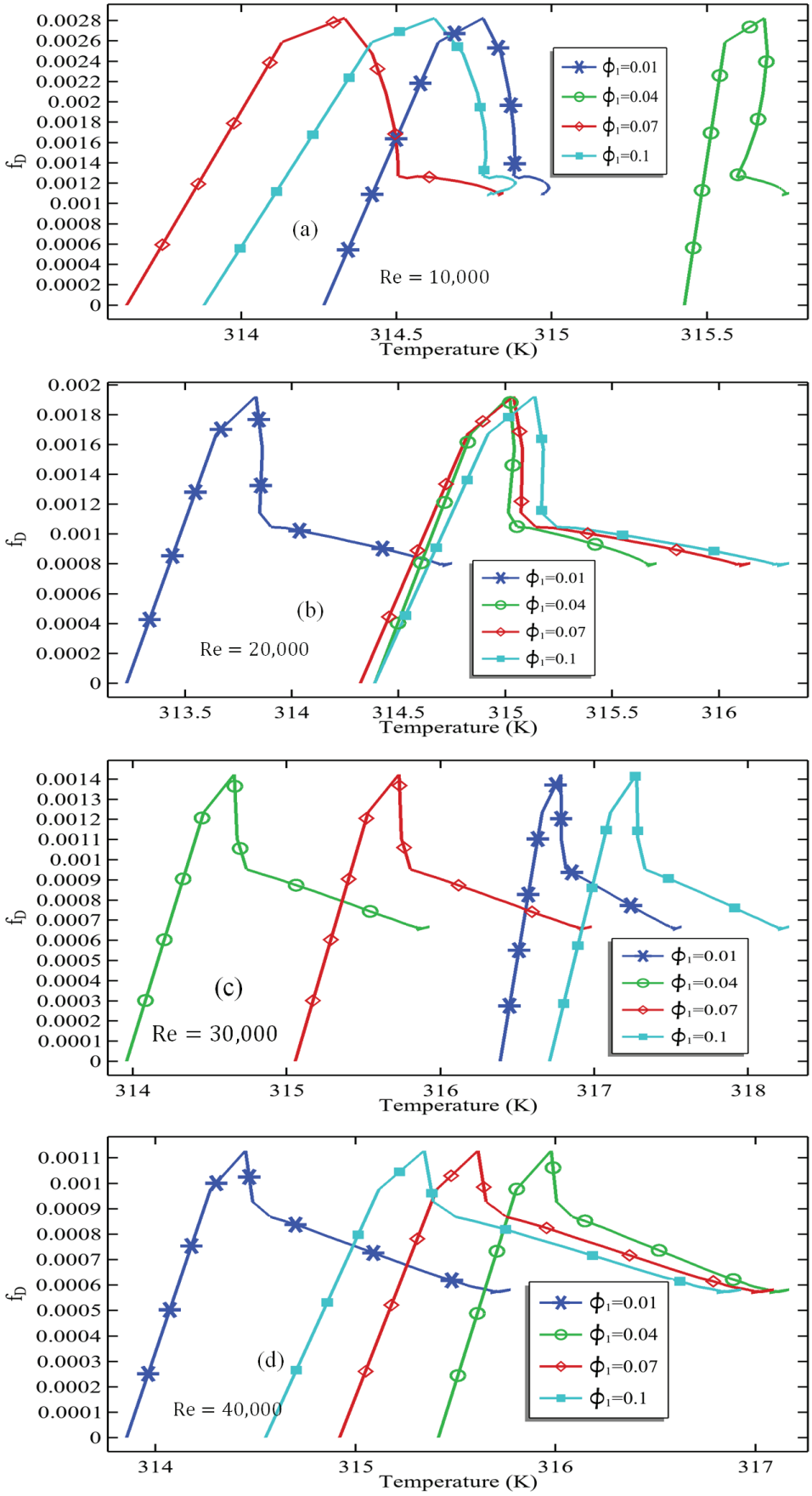

Figure 13. Temperature and the friction factor along the length of the channel when $\phi_2 = 0.01$.

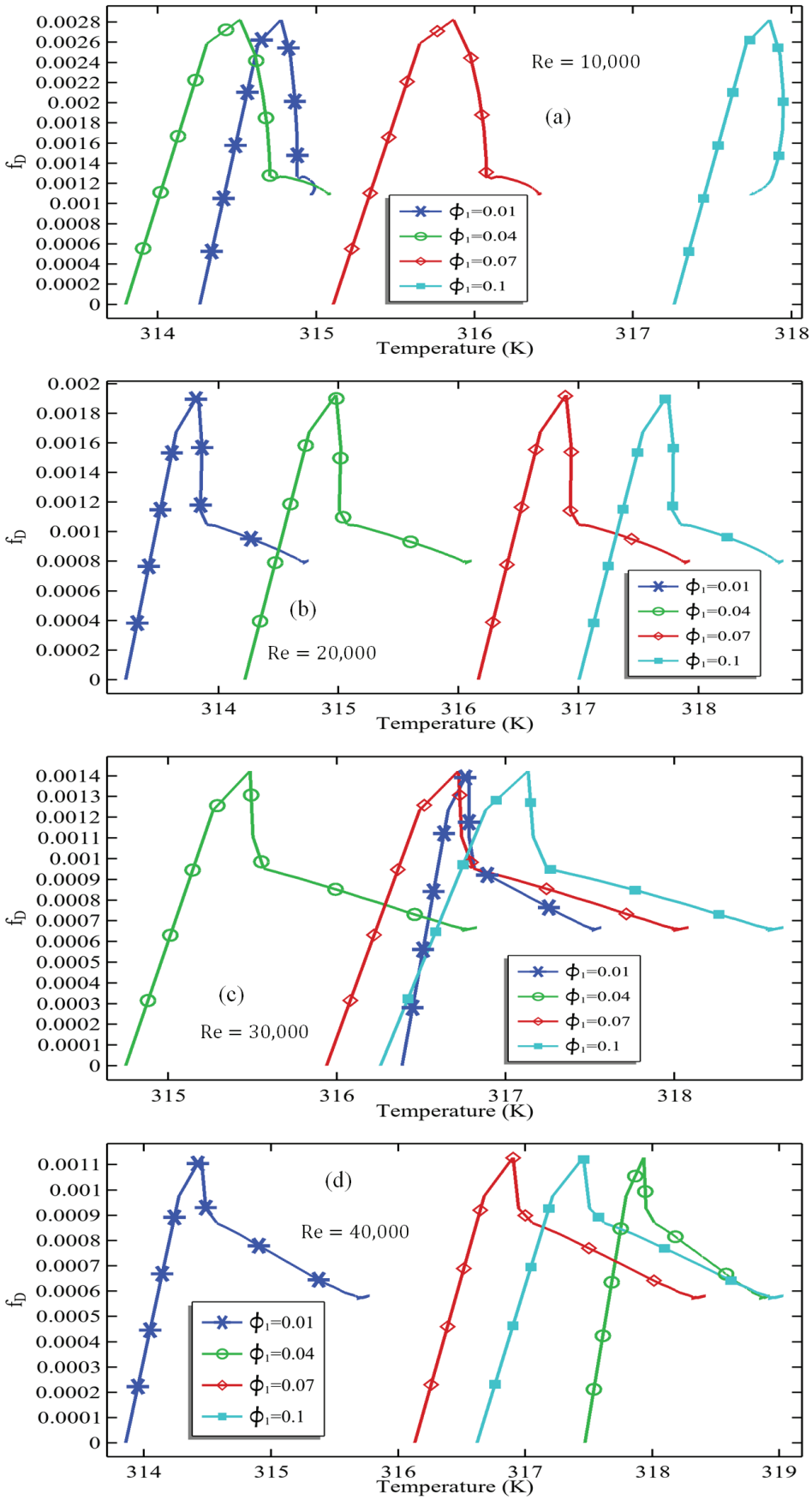

Figure 14(a-d). Temperature and the friction factor along the length of the channel when $\phi_1 = 0.01$.

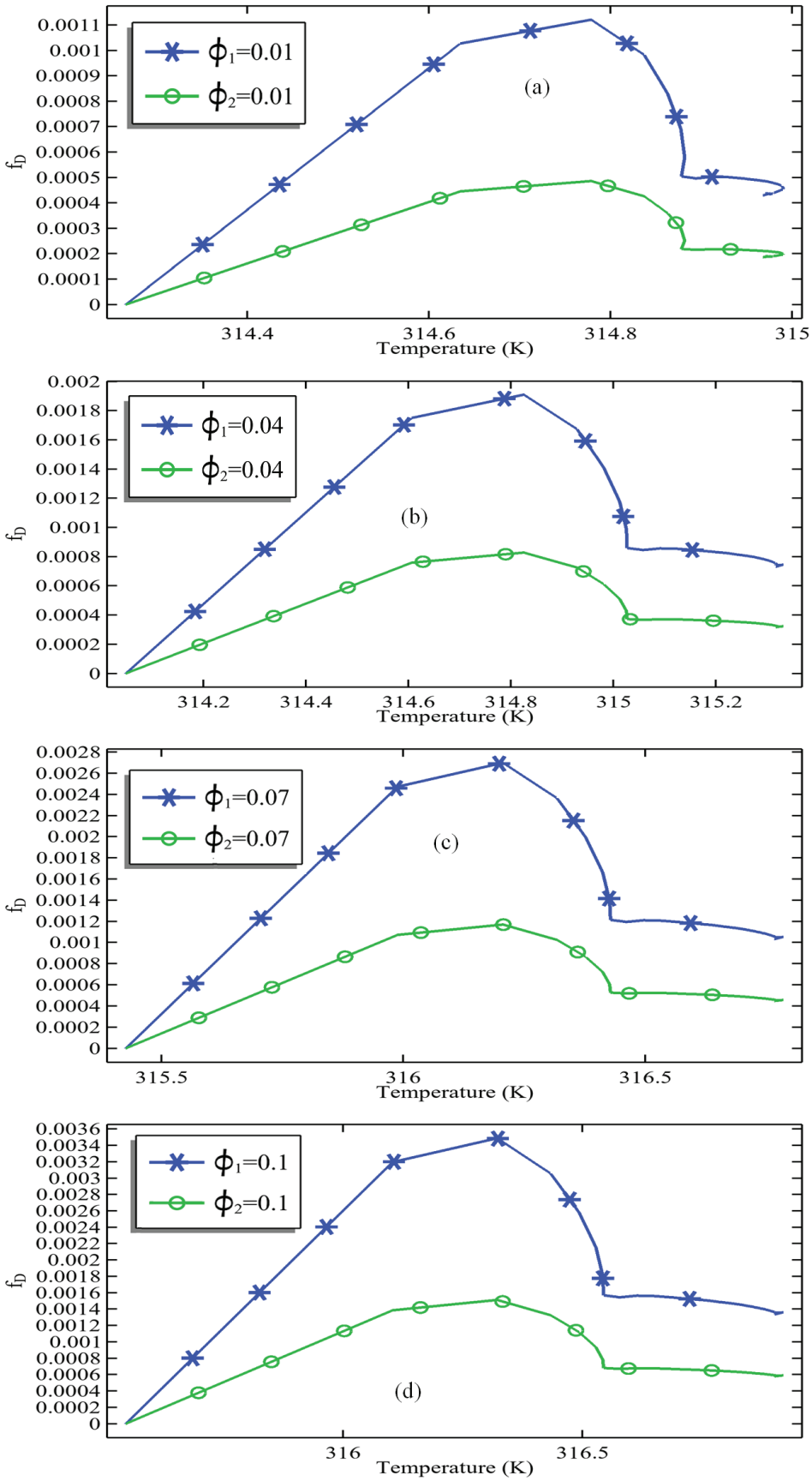

Figure 15(a-d). Comparison of friction factor between the aluminum oxide and the copper keeping both the volume fraction equal at Re=10,000.

proves challenging, underscoring the indispensable role of Reynolds number adjustments in elucidating this complex phenomenon.

Figures 15(a-d) present a comprehensive comparative analysis of both the Darcy friction factor and temperature, specifically examining the influence of various factors on these critical parameters. The study maintains a constant Reynolds number while considering equal volume fractions of aluminum oxide and copper nanoparticles. Notably, the results presented in Figure. 15(a-d) reveal an intriguing trend: the Darcy friction factor for aluminum oxide consistently exceeds that of copper. This discrepancy can be attributed to the greater density of aluminum oxide compared to copper, a pivotal factor affecting the flow dynamics within the channel. Additionally, it's essential to clarify that the temperature values indicated along the x-axis of these figures represent the overall temperature distribution across the entire channel length. The temperature profile is instrumental in understanding how heat dissipates and transfers within the channel under varying conditions. Of particular significance, we can observe a noteworthy relationship between the total volume fraction of the channel and the resulting temperature. As the total volume fraction increases, there is a corresponding escalation in temperature along the length of the channel. This finding underscores the importance of considering the impact of volume fraction variations on thermal behavior and serves as valuable insight for optimizing heat transfer processes within this system.

Physical reasons: The decline in the friction factor beyond certain temperatures in Figures 14(a-d) and 15(a-d) is attributed to the interaction between fluid viscosity, thermal expansion, and flow dynamics. As the temperature increases, the viscosity of the hybrid nanofluid decreases, reducing flow resistance and, consequently, the friction factor at the channel edges. Additionally, rising fluid temperatures lead to thermal expansion, which decreases the fluid density and further reduces flow resistance. The maximum friction factor occurs at a peak where there is an optimal balance between the fluid's momentum and its decreasing viscosity. Beyond this peak, the reduction in viscosity dominates, causing the friction factor to decline. Higher Reynolds numbers also contribute to increased fluid velocity and turbulence, enhancing momentum forces and mitigating the effect of the friction factor. This behavior remains consistent across varying volume fractions of copper and alumina, due to their distinct thermal conductivities and densities.

CONCLUSION

In the course of our present investigation, we meticulously scrutinized the behavior of a three-dimensional L-shaped channel as it accommodated the flow of a hybrid mixture containing aluminum oxide and copper. Our primary focus revolved around the intricate dynamics of turbulent forced convection. This endeavor was underpinned by the application of the $\kappa - \varepsilon$ turbulence model, which we expertly integrated with energy equations. The entire computational framework was adeptly executed through the Finite Element Method within the powerful COMSOL Multiphysics 5.6 platform. Our study encompassed a comprehensive spectrum of scenarios, each meticulously engineered to explore various volume fractions for both nanoparticles. Specifically, we considered volume fractions of 0.01, 0.04, 0.07, and 0.1 while subjecting the fluid to a range of Reynolds numbers spanning from 10,000 to 40,000. To ensure the robustness of our findings, we conducted a rigorous mesh-independent study and systematically validated our results against established correlations for the local Nusselt number. The culmination of our extensive numerical investigations unveiled several noteworthy insights and observations.

- The minimum temperature initially decreases with an increasing aluminum oxide volume fraction, followed by an increase. This behavior is specifically observed at Reynolds numbers ranging from 10,000 to 30,000 and at copper volume fractions of 0.01 and 0.04
- The addition of copper enhances the minimum temperature at both edges of the channel. Furthermore, an increase in Reynolds number consistently raises the minimum temperature across all scenarios in our simulation.
- Notably, increasing the copper volume fraction consistently improves the minimum temperatures at the channel's two edges.
- Applying the linear regression procedure, it was found that the average temperature at the outlet depended solely on the Reynolds number. It was observed that the average temperature increased by a value of 0.0000132 for each unit increase in the Reynolds number. Using this correlation for the average temperature at the outlet, the minimum and maximum absolute errors achieved were 0.005188 and 1.6, respectively.
- In comparing the local Nusselt numbers for aluminum oxide and copper, a outstanding observation emerges: the local Nusselt number for aluminum oxide surpasses that of copper by a factor of approximately 10.
- Applying the multiple linear regression procedure, a linear regression equation for the average Nusselt number was derived. According to this equation, the average Nusselt number at the outlet depends solely on the copper volume fraction and the Reynolds number. Using this correlation, it was determined that the average Nusselt number at the outlet increases by 13.492917 and 0.002245559 when one unit of volume fraction and Reynolds number is increased, respectively. By utilizing this linear regression, a minimum error of 0.36810583 and a maximum error of 1.6 can be achieved.
- The Darcy friction factor shows a clear pattern, increasing along the channel length to a maximum before gradually decreasing. This trend is consistent across all cases.

The factor's response to volume fraction changes in copper and aluminum oxide is non-deterministic, meaning it may either increase or decrease. Moreover, the Darcy friction factor decreases as the Reynolds number rises.

NOMENCLATURE

U	Velocity field
u	x-component of velocity
v	y-component of velocity
w	z-component of velocity
$\nabla = < \frac{\partial}{\partial x}, \frac{\partial}{\partial y}, \frac{\partial}{\partial z} >$	Gradient operator
I	Identity vector
P	Pressure
μ_{nf}	Hybrids nanofluids viscosity
μ_T	Turbulent viscosity (Eddy Viscosity)
κ	Turbulent kinetic energy
p_κ	Kinetic energy production
ε	Energy Dissipation rate
L_x	Length along the x-axis
L_y	Length along the y-axis
L_z	Length along the z-axis
u_{in}	Inlet velocity
Re	Reynolds number
κ_0	Initial kinetic energy
ε_0	Initial dissipation rate
I_T	Initial turbulence intensity
L_T	Initial turbulence length
n	Normal vector on the boundary
p_{out}	Pressure at outlet
T_h	Hot temperature
δ_w^+	Wall distance
T_c	Cold temperature
$\kappa_v, \sigma_\kappa, \sigma_\varepsilon, c_\mu, c_{\varepsilon 1}, c_{\varepsilon 2}$	Model parameters
τ_w	Wall shear stress
T	Transpose
U_{mean}	Mean velocity
Avg	Average
Nu	Nusselt number
Pr	Prandtl Number
Q	Heat flux
X	x-axis
Y	y-axis
Z	z-axis

AUTHORSHIP CONTRIBUTIONS

Authors equally contributed to this work.

DATA AVAILABILITY STATEMENT

The authors confirm that the data that supports the findings of this study are available within the article. Raw data that support the finding of this study are available from the corresponding author, upon reasonable request.

CONFLICT OF INTEREST

The author declared no potential conflicts of interest with respect to the research, authorship, and/or publication of this article.

ETHICS

There are no ethical issues with the publication of this manuscript.

STATEMENT ON THE USE OF ARTIFICIAL INTELLIGENCE

Artificial intelligence was not used in the preparation of the article

REFERENCES

[1] Akbari OA, Safaei MR, Goodarzi M, Akbar NS, Zarringhalam M, Shabani GA, et al. A modified two-phase mixture model of nanofluid flow and heat transfer in a 3-D curved microtube. Adv Powder Technol 2016;27:2175–2185. [CrossRef]

[2] Allehiany FM, Memon AA, Memon MA, Fenta A. Maximizing electrical output and reducing heat-related losses in photovoltaic thermal systems with a thorough examination of flow channel integration and nanofluid cooling. Sci Rep 2023;13:16961. [CrossRef]

[3] Mashayekhi R, Khodabandeh E, Akbari OA, Toghraie D, Bahiraei M, Gholami M. CFD analysis of thermal and hydrodynamic characteristics of hybrid nanofluid in a newly designed sinusoidal double-layered microchannel heat sink. J Therm Anal Calorim 2018;134:2305–2315. [CrossRef]

[4] Mashayekhi R, Khodabandeh E, Bahiraei M, Bahrami L, Toghraie D, Akbari OA. Application of a novel conical strip insert to improve the efficacy of water–Ag nanofluid for utilization in thermal systems: a two-phase simulation. Energy Convers Manag 2017;151:573–586. [CrossRef]

[5] Darzi AAR, Afrouzi HH, Khaki M, Abbasi M. Unconstrained melting and solidification inside rectangular enclosure. J Fundam Appl Sci 2015;7:436–451. [CrossRef]

[6] Rabienataj Darzi AA, Afrouzi HH, Alizadeh E, Shokri V, Farhadi M. Numerical simulation of heat and mass transfer during absorption of hydrogen in metal hydride tank. Heat Transf Asian Res 2017;46:75–90. [CrossRef]

[7] Hassanzadeh Afrouzi H, Moshfegh A, Farhadi M, Sedighi K. Dissipative particle dynamics simulation hydrated Nafion EW 1200 as fuel cell membrane in nanoscopic scale. Chall Nano Micro Scale Sci Technol 2016;5:44–53. [CrossRef]

[8] Akbari OA, Hassanzadeh Afrouzi H, Marzban A, Toghraie D, Malekzade H, Arabpour A. Investigation of volume fraction of nanoparticles effect and aspect ratio of the twisted tape in the tube. J Therm Anal Calorim 2017;129:1911−1922. [CrossRef]
[9] Sajid T, Ayub A, Shah SZH, Jamshed W, Eid MR, Tag El Din ESM, et al. Trace of chemical reactions accompanied with Arrhenius energy on ternary hybridity nanofluid past a wedge. Symmetry 2022;14:1850. doi: 10.3390/sym14091850. [CrossRef]
[10] Hassanzadeh Afrouzi H, Rabienataj Darzi AA, Delavar MA, Abouei Mehrizi A. Pulsating flow and heat transfer in a helical tube with constant heat flux. Int J Adv Ind Eng 2013;1:36−39.
[11] Akram M, Memon AA, Memon MA, Obalalu AM, Khan U. Investigation of a two-dimensional photovoltaic thermal system using hybrid nanofluids and a rotating cylinder. Nanoscale Adv 2023;5:5529−5542. [CrossRef]
[12] Memon AA, Memon MA, Haque MM. Numerical investigation of electrical efficiency with the application of hybrid nanofluids for photovoltaic thermal systems contained in a cavity channel. J Math 2023;2023:1466881. [CrossRef]
[13] Memon AA, Khan WA, Muhammad T. Numerical investigation of photovoltaic thermal energy efficiency improvement using the backward step containing Cu-Al2O3 hybrid nanofluid. Alexandria Eng J 2023;75:391−406. [CrossRef]
[14] Alghamdi M, Memon AA, Muhammad T, Ali MR. A numerical investigation of a photovoltaic thermal system contained a trapezoidal channel with transport of silver and titanium oxide using the water as base fluids. Case Stud Therm Eng 2023;47:103056. [CrossRef]
[15] Ramzan M, Shamshad U, Rehman S, Saeed A, Kumam P, Watthayu W. Computation of MHD flow of three-dimensional mixed convection non-Newtonian viscoelastic fluid with the physical aspect of gyrotactic microorganism. Waves Random Complex Media 2022:1−23. [CrossRef]
[16] Abraham JD, Mohanraj M. Thermodynamic performance of automobile air conditioners working with R430A as a drop-in substitute to R134a. J Therm Anal Calorim 2019;136:2071−2086. [CrossRef]
[17] Choi SUS, Eastman JA. Enhancing thermal conductivity of fluids with nanoparticles. In: Siginer DA, Wang HP, editors. Developments and applications of non-Newtonian flows. New York: ASME; 1995. p. 99−105. [CrossRef]
[18] Tiwari RK, Das MK. Heat transfer augmentation in a two-sided lid-driven differentially heated square cavity utilizing nanofluids. Int J Heat Mass Transf 2007;50:2002−2018. [CrossRef]
[19] Ramzan M, Rehman S, Junaid MS, Saeed A, Kumam P, Watthayu W. Dynamics of Williamson Ferro-nanofluid due to bioconvection in the portfolio of magnetic dipole and activation energy over a stretching sheet. Int Commun Heat Mass Transf 2022;137:106245. [CrossRef]
[20] Ramzan M, Shah Z, Kumam P, Khan W, Watthayu W, Kumam W. Bidirectional flow of MHD nanofluid with Hall current and Cattaneo-Christove heat flux toward the stretching surface. PLoS One 2022;17:e0264208. [CrossRef]
[21] Asadi M, Asadi A, Aberoumand S. An experimental and theoretical investigation on the effects of adding hybrid nanoparticles on heat transfer efficiency and pumping power of an oil-based nanofluid as a coolant fluid. Int J Refrig 2018;89:83−92. [CrossRef]
[22] Rashad AM, Armaghani T, Chamkha AJ, Mansour MA. Entropy generation and MHD natural convection of a nanofluid in an inclined square porous cavity: effects of a heat sink and source size and location. Chin J Phys 2018;56:193−211. [CrossRef]
[23] Gorla RSR, Siddiqa S, Mansour MA, Rashad AM, Salah T. Heat source/sink effects on a hybrid nanofluid-filled porous cavity. J Thermophys Heat Transf 2017;31:847−857. [CrossRef]
[24] Han ZH, Yang B, Kim SH, Zachariah MR. Application of hybrid sphere/carbon nanotube particles in nanofluids. Nanotechnology 2007;18:105701. [CrossRef]
[25] Botha SS, Ndungu P, Bladergroen BJ. Physicochemical properties of oil-based nanofluids containing hybrid structures of silver nanoparticles supported on silica. Ind Eng Chem Res 2011;50:3071−3077. [CrossRef]
[26] Jana S, Salehi-Khojin A, Zhong WH. Enhancement of fluid thermal conductivity by the addition of single and hybrid nano-additives. Thermochim Acta 2007;462:45−55. [CrossRef]
[27] Ho CJ, Huang JB, Tsai PS, Yang YM. Preparation and properties of hybrid water-based suspension of Al2O3 nanoparticles and MEPCM particles as functional forced convection fluid. Int Commun Heat Mass Transf 2010;37:490−494. [CrossRef]
[28] Ho CJ, Huang JB, Tsai PS, Yang YM. Water-based suspensions of Al2O3 nanoparticles and MEPCM particles on convection effectiveness in a circular tube. Int J Therm Sci 2011;50:736−748. [CrossRef]
[29] Suresh S, Venkitaraj KP, Selvakumar P, Chandrasekar M. Synthesis of Al2O3−Cu/water hybrid nanofluids using two step method and its thermo physical properties. Colloids Surf A Physicochem Eng Asp 2011;388:41−48. [CrossRef]
[30] Baghbanzadeh M, Rashidi A, Rashtchian D, Lotfi R, Amrollahi A. Synthesis of spherical silica/multiwall carbon nanotubes hybrid nanostructures and investigation of thermal conductivity of related nanofluids. Thermochim Acta 2012;549:87−94. [CrossRef]
[31] Paul G, Philip J, Raj B, Das PK, Manna I. Synthesis, characterization, and thermal property measurement of nano-Al95Zn05 dispersed nanofluid prepared by a two-step process. Int J Heat Mass Transf 2011;54:3783−3788. [CrossRef]

[32] Baby TT, Ramaprabhu S. Synthesis and nanofluid application of silver nanoparticles decorated graphene. J Mater Chem 2011;21:9702–9709. [CrossRef]
[33] Baby TT, Ramaprabhu S. Experimental investigation of the thermal transport properties of a carbon nanohybrid dispersed nanofluid. Nanoscale 2011;3:2208–2214. [CrossRef]
[34] Baby TT, Ramaprabhu S. Synthesis of silver nanoparticle decorated multiwalled carbon nanotubes-graphene mixture and its heat transfer studies in nanofluid. AIP Adv 2013;3:012111. [CrossRef]
[35] Armaghani T, Sadeghi MS, Rashad AM, Mansour MA, Chamkha AJ, Dogonchi AS, et al. MHD mixed convection of localized heat source/sink in an Al2O3-Cu/water hybrid nanofluid in L-shaped cavity. Alexandria Eng J 2021;60:2947–2962. [CrossRef]
[36] Selimefendigil F, Öztop HF. Combined effects of double rotating cones and magnetic field on the mixed convection of nanofluid in a porous 3D U-bend. Int Commun Heat Mass Transf 2020;116:104703. [CrossRef]
[37] Ghasemi K, Siavashi M. Three-dimensional analysis of magnetohydrodynamic transverse mixed convection of nanofluid inside a lid-driven enclosure using MRT-LBM. Int J Mech Sci 2020;165:105199. [CrossRef]
[38] Ganesh NV, Javed S, Al-Mdallal QM, Kalaivanan R, Chamkha AJ. Numerical study of heat generating γ Al2O3–H2O nanofluid inside a square cavity with multiple obstacles of different shapes. Heliyon 2020;6:e05752. [CrossRef]
[39] Afrand M, Pordanjani AH, Aghakhani S, Oztop HF, Abu-Hamdeh N. Free convection and entropy generation of a nanofluid in a tilted triangular cavity exposed to a magnetic field with sinusoidal wall temperature distribution considering radiation effects. Int Commun Heat Mass Transf 2020;112:104507. [CrossRef]
[40] Nath R, Murugesan K. Numerical investigation of double-diffusive mixed convection of Fe3O4/Cu/Al2O3-water nanofluid flow through a backward-facing-step channel subjected to magnetic field. Int J Numer Method Heat Fluid Flow 2021;31:1883–1913. [CrossRef]
[41] Miroshnichenko IV, Sheremet MA. Radiation effect on conjugate turbulent natural convection in a cavity with a discrete heater. Appl Math Comput 2018;321:358–371. [CrossRef]
[42] Miroshnichenko IV, Sheremet MA. Turbulent natural convection combined with thermal surface radiation inside an inclined cavity having local heater. Int J Therm Sci 2018;124:122–130. [CrossRef]
[43] Alsabery AI, Sheremet MA, Chamkha AJ, Hashim I. Forced convection of turbulent flow into the wavy parallel channel. J Therm Anal Calorim 2022;147:11183–11194. [CrossRef]
[44] Iachachene F, Haddad Z, Arıcı M, Abu-Nada E, Sheremet MA. The effect of nano encapsulated phase change materials and nanoparticles on turbulent heat transport: A conical diffuser scenario. J Energy Storage 2022;52:104703. [CrossRef]
[45] Miroshnichenko IV, Sheremet MA. Turbulent natural convection heat transfer in rectangular enclosures using experimental and numerical approaches: A review. Renew Sustain Energy Rev 2018;82:40–59. [CrossRef]
[46] Salhi H, Chafai N. Evaluation of the thermal conductivity of nanofluids using statistical analysis methods. Nanosci Technol Int J 2022;13:29–39. [CrossRef]
[47] Baiti A, Salhi H, Chafai N. Numerical investigation of turbulent mixed convection in a round bottom flask using a hybrid nanofluid. Adv Mech Eng 2023;15:16878132231195022. [CrossRef]
[48] Salhi H, Chafai N. Numerical simulation of heat transfer in a square cavity with a heater and cooler using hybrid nanofluid and random temperature. Nanosci Technol Int J 2023;14:47–59.
[49] Salhi H, Chafai N, Moussaoui I, Mahamdi A. Influence of hybrid nanofluids and source configuration on natural convection in square cavity. Nanosci Technol Int J 2024;15:35–47. [CrossRef]
[50] Dittus FW, Boelter LMK. Heat transfer in automobile radiators of the tubular type. Int Commun Heat Mass Transf 1985;12:3–22. [CrossRef]
[51] Gawande VB, Dhoble AS, Zodpe DB, Chamoli S. Experimental and CFD investigation of convection heat transfer in solar air heater with reverse L-shaped ribs. Sol Energy 2016;131:275–295. [CrossRef]
[52] Alqarni MS, Memon AA, Anwaar H, Usman, Muhammad T. The forced convection analysis of water alumina nanofluid flow through a 3D annulus with rotating cylinders via κ–ε turbulence model. Energies 2022;15:6730. [CrossRef]
[53] Grégoire G. Multiple linear regression. EAS Publ Ser 2014;66:45–72. [CrossRef]
[54] Jobson JD. Multiple linear regression. In: Applied multivariate data analysis: regression and experimental design. New York: Springer; 1991. p. 219–398. [CrossRef]
[55] Elhag SH, Memon AA, Memon MA, Bhatti K, Jacob K, Alzahrani S, et al. Analysis of forced convection with hybrid Cu-Al2O3 nanofluids injected in a three-dimensional rectangular channel containing three perpendicular rotating blocks with turbulent modeling. J Nanomater 2022;2022:2464191. [CrossRef]
[56] Taler D, Taler J. Simple heat transfer correlations for turbulent tube flow. E3S Web Conf 2017;13:02008. [CrossRef]